



DISTRIBUTION STATEMENT A
Approved for public release
Distribution Unlimited

*EVALUATION OF SATELLITE MICROWAVE DERIVED
SURFACE TEMPERATURE ALGORITHMS
FOR THE PERIOD AUGUST 1996 TO FEBRUARY 1997*

THESIS

Charles H. Harris
Captain, USAF

AFIT/GM/ENP/98M-04

DTIC QUALITY INSPECTED 4

DEPARTMENT OF THE AIR FORCE
AIR UNIVERSITY

AIR FORCE INSTITUTE OF TECHNOLOGY

Wright-Patterson Air Force Base, Ohio

19980408 127

AFIT/GM/ENP/98M-04

*EVALUATION OF SATELLITE MICROWAVE DERIVED
SURFACE TEMPERATURE ALGORITHMS
FOR THE PERIOD AUGUST 1996 TO FEBRUARY 1997*

THESIS

Charles H. Harris
Captain, USAF

AFIT/GM/ENP/98M-04

Approved for public release; distribution unlimited

The views expressed in this thesis are those of the author
and do not reflect the official policy or position of the
Department of Defense or the U.S. Government.

AFIT/GM/ENP/98M-04

***EVALUATION OF SATELLITE MICROWAVE DERIVED
SURFACE TEMPERATURE ALGORITHMS
FOR THE PERIOD AUGUST 1996 TO FEBRUARY 1997***

THESIS

Presented to the Faculty of the Graduate School of Engineering

of the Air Force Institute of Technology

Air University

Air Education and Training Command

In Partial Fulfillment of the

Requirements for the Degree of

Master of Science in Meteorology

Charles H. Harris, B.S., M.B.A.

Captain, USAF

March 1998

Approved for public release; distribution unlimited

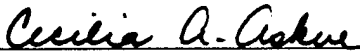
**EVALUATION OF SATELLITE MICROWAVE DERIVED
SURFACE TEMPERATURE ALGORITHMS
FOR THE PERIOD AUGUST 1996 TO FEBRUARY 1997**

Charles H. Harris, B.S., M.B.A.
Captain, USAF

Approved:


Maj. Clifton E. Dungey, Chairman

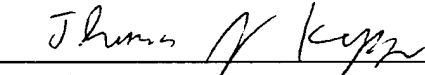
6 Mar 98
date


Lt. Col. Cecilia A. Askue

5 Mar 98
date


Maj. Derrill T. Goldizen

6 Mar 98
date


Dr. Thomas J. Kopp

18 Feb 98
date

Acknowledgments

First and foremost I must express gratitude to my Lord and Savior. During all the lonely, anxiety, pressure, and victory filled moments of this research He was always there to comfort and guide me. I would like to next express my thanks to the AF and AFIT for allowing me the opportunity to go to a school with a combined technological-military focus. I will no doubt give my country a higher level of service because of AFIT.

I certainly have to thank my advisor for all his guidance and especially the freedom to work, flounder, and achieve on my own. I would also like to thank my fellow classmates in GM-98M who helped me immensely in my time here at AFIT. I especially wish to thank a former AFIT student who paved the way for this body of work. Capt. Ron Comoglio did great original work for me to build on and obtain good results. My success is a reflection of his efforts in laying a solid foundation. I must also thank Ron Wall at AFCCC. He provided outstanding support, especially in the area of short notice requests.

My kids, Caitlin (six) and Alex (two), probably won't remember too much of AFIT. But I will never forget my daughter's understanding of Daddy's hard work. And now I must express how grateful I am to the most important aspect of my life of this world - my wife Sheryl. With her tremendous support through another difficult phase of our lives, she has again demonstrated how much a spouse can love another spouse. She has shown me how one person truly supports another. On the eve of our tenth anniversary, I pray I get the opportunity to demonstrate how much I love her as she has done on such a grand scale

in the past ten years, and especially in the past year and a half. I am continually grateful to the Lord for the greatest blessing in my life – my wife and best friend Sheryl.

Charles H. Harris

Table of Contents

	Page
<i>Acknowledgments</i>	ii
<i>List of Figures</i>	vii
<i>List of Tables</i>	viii
<i>Abstract</i>	ix
<i>I. Introduction</i>	1
Chapter Overview	1
Introduction	1
Background	2
Global Surface Temperatures	2
Passive Microwave Radiometry	2
Defense Meteorological Satellite Program	2
Algorithms	2
Problem and Assumptions	3
Research Scope and General Approach	4
Research Results	4
Summary	5
<i>II. Background</i>	6
Chapter Overview	6
Introduction	6
Electromagnetic Radiation	7
Non-Blackbody and Land Effects	12
Remote Sensing History	14
DMSP and the SSMI	16
Atmospheric Effects	20
Antenna Theory	25
Temperature Retrieval Technique – Statistical Inversion Method	28
Calibration/Validation (CV) Algorithm and FORTRAN Code	31

Table of Contents

	Page
Temperature from Sensor Microwave Imager (TS) Algorithm and FORTRAN Code.....	33
Applications of SSM/I data.....	35
Sources of Error.....	36
Remote Sensing of Land Surface Temperatures - Literature Review	37
Summary	38
 <i>III. Methodology</i>	 39
Chapter Overview.....	39
Building on Past Work at AFIT	39
Data Sources and Description	40
Data Comparison Process.....	43
Comparison Methods.....	48
Statistics	49
Data Stratification	50
Summary	51
 <i>IV. Results Analysis</i>	 52
Chapter Overview.....	52
Data Sets.....	52
Algorithm Production.....	53
Data Pair Sample Sizes	55
Bias	56
Root Mean Square Error	59
Summary	60
 <i>V. Summary and Recommendations</i>	 61
Summary	61
Data Processing Recommendations.....	61
Research Recommendations.....	62

Table of Contents

	Page
<i>Appendix A: Summer CONUS Matches</i>	63
<i>Appendix B: Fall CONUS Matches</i>	64
<i>Appendix C: Winter CONUS Matches</i>	65
<i>Appendix D. Summer Bosnian Matches</i>	66
<i>Appendix E. Fall Bosnian Matches</i>	67
<i>Appendix F. Winter Bosnian Matches</i>	68
<i>Appendix G. Summer Korean Matches</i>	69
<i>Appendix H. Fall Korean Matches</i>	70
<i>Appendix I. Winter Korean Matches</i>	71
<i>Appendix J: Summer Saudi Arabian Matches</i>	72
<i>Appendix K: Fall Saudi Arabian Matches</i>	73
<i>Appendix L: Winter Saudi Arabian Matches</i>	74
<i>Bibliography</i>	75
<i>Vita</i>	77

List of Figures

Figure	Page
1. Wavelength Distribution of Earth with Highlighted Microwave Region	7
2. Rayleigh-Jeans Approximation to the Planck Function.....	12
3. SSM/I Global Coverage	17
4. Percentage Transmission Through Clear Atmosphere in Vertical Direction with SSM/I frequencies.	18
5. SSM/I Scan Geometry	19
6. Satellite Radiometer Sources of Radiation	21
7. Polar Stereographic Northern Hemisphere Grid.....	27
8. Data Comparison Process.....	44
9. Polar Steographic Grid over Malmstrom AFB (GFA)	48

List of Tables

Table	Page
1. Brightness Temperatures for the 19 GHz SSM/I Frequency.	25
2. CV Land Surface Temperature Algorithms.	32
3. TS Land Surface Temperature Algorithms for DMSP F13	34
4. Comparison of Comoglio and Harris results for CONUS Aug 96.	41
5. SSM/I Raw Data Files.....	42
6. Ground Station Data Formats.....	42
7. Output from Satellite Observation Time Program.....	45
8. Output from Surface Temperature Algorithm Programs.	45
9. Output from Ground Station Program.....	46
10. Output from Matching Program.....	47
11. Surface Temperature Production Rate (%) for the Temperature from Sensor Microwave Imager (TS) and Calibration/Validation (CV) Algorithms.....	53
12. Number of Data Pairs for the Temperature from Sensor Microwave Imager (TS) and Calibration/Validation (CV) Algorithms.....	55
13. Bias (K) for the Temperature from Sensor Microwave Imager (TS) and Calibration/Validation (CV) Algorithms.....	57
14. RMSE (K) for the Temperature from Sensor Microwave Imager (TS) and Calibration/Validation (CV) Algorithms.....	59

Abstract

The Air Force Weather Agency (AFWA) has two operational algorithms that derive surface temperatures from microwave observations taken by the Special Sensor Microwave Imager (SSM/I) which rides aboard space platforms of the Defense Meteorological Satellite Program (DMSP). The algorithm called Temperature from Satellite Microwave Imager (TS) is used to forecast surface temperatures and analyze global cloud coverage. The second algorithm is fittingly called Calibration/Validation (CV), as it was the algorithm used to calibrate and validate the first SSM/I back in 1987. Multiple linear regression defined the algorithms from empirically gathered brightness temperatures and simultaneous surface temperatures. The key questions at hand are how much data do these algorithms produce and how accurate is it.

The current thesis answered the above questions with a multi-seasonal comparative study over four locations. The study matched algorithm outputs to conventional weather station temperature readings to produce data pairs. Over 13,300 data pairs were generated from the 1996 summer and fall and 1996-1997 winter for the Continental United States (CONUS), Bosnia, Korean Peninsula, and Saudi Arabia.

The results show TS produced on average 7 % more surface temperatures than CV. CV met AFWA's accuracy criteria 16 % more often than TS. However, CV was only 1.0 degree Celsius more accurate than TS on average. The study also generated bias tables for all locations and seasons.

**EVALUATION OF SATELLITE MICROWAVE DERIVED
SURFACE TEMPERATURE ALGORITHMS
FOR THE PERIOD AUGUST 1996 TO FEBRUARY 1997**

I. Introduction

Chapter Overview

After a general introduction to the problem of inadequate amounts of global surface temperatures, the chapter introduces the concept of remote sensing, specifically microwave remote sensing. The background section outlines the space platform, instrument, and algorithms of concern in this study. After the specific research problem is defined and some assumptions made, the scope and general approach of the research are explained. Finally, this chapter provides the general results of the research.

Introduction

One special attribute of the human species is the ability to extend our natural five senses, especially sight, with tools of our own creation. By creating sensors that detect or see beyond the visible part of the electromagnetic spectrum, we learn more about our environment. One class of these sensors resides on earth-orbiting satellites; they detect a totally different portion of the electromagnetic spectrum – microwaves. These microwave observations determine many atmospheric parameters, including surface temperature. As a result, humans extend their natural senses to see global surface temperatures from space.

Background

Even in modern times, the ability to accurately measure global surface temperatures is a problem. The conventional weather station network does not cover remote regions. The data sparseness affects atmospheric models that require a fine data analysis to accurately predict the future state of the atmosphere. As pointed out by McClatchey and Greenwood (1996), the timeliness, specificity, and responsiveness requirements of the military for weather information greatly exceed those of the civilian world. Remote sensing from space-borne platforms is one answer to the data sparseness problem.

One method to improve the analysis of global surface or land temperatures is through the remote observation of earth's microwave emissions sensed from satellites – a process referred to as Passive Microwave Radiometry (PMR). Space-borne PMR has been in existence since the early 1960's (Ulaby, 1981). The primary advantage of using the microwave portion of the electromagnetic (EM) spectrum (versus thermal or visible) is the ability to see through clouds.

There are many types of remote sensing satellites. One such system is the Defense Meteorological Satellite Program (DMSP). The type of microwave sensor aboard the DMSP satellites, called Special Sensor Microwave/Imager (SSM/I), has been operational since 1987. In April 1997, the US Air Force launched the latest DMSP satellite, F14, from Vandenberg AFB, California (Cooper, 1997).

Air Force Weather Agency (AFWA) has two operational algorithms for calculating surface temperatures derived from microwave emissions sensed aboard DMSP space platforms. The first algorithm, called Temperature from Sensor Microwave Imager

(TMPSMI or TS), provides input for the global surface temperature model and the global cloud coverage model (Kopp, 1995). The second algorithm, fittingly called Calibration/Validation (CV), was the algorithm used to calibrate and validate the first SSM/I in 1987.

Problem and Assumptions

AFWA's atmospheric models require an accurate global analysis of surface temperatures in order to correctly specify and forecast global cloud coverage. In addition, military forecasters need near real time surface temperatures from data sparse or denied territory. A current temperature analysis aids in model verification and temperature forecasts. Among many other military uses, these surface temperature applications are critical for the use of precision guided munitions – key tools in the application of today's US military power.

The problem addressed in this paper is the performance of the TS and CV algorithms. Which algorithm produces more temperatures and which one is more accurate? No research to date has extensively compared the two algorithms.

There are two assumptions from the outset. First, the weather station temperature observations are truth data. There was no attempt made to analyze the accuracy of the station data. Secondly, the algorithms contain correct computer code. This study does not aim to improve the algorithms, rather just compare their outputs.

Research Scope and General Approach

DMSP SSM/I data from the F13 satellite was the only microwave data source in the study. An initial study occurred in the fall of 1996 but portions needed reaccomplishment due to data problems. Furthermore, the comparison needs spatial and temporal expansion (Comoglio, 1997).

SSM/I and weather station data were gathered for summer 1996, fall 1996, and winter (Jan-Feb) 97. The study covers the land regions of the CONUS and other regions of interest to the US military: Korea, Saudi Arabia, and Bosnia.

After reformatting the raw SSM/I data, both algorithms were run for the areas of interest. The production counts were then obtained. The raw station data was also reformatted. Then, a program matched the SSM/I and weather station data by location and time to create data pairs. Finally, descriptive statistics were generated and analyzed on production, tendency, and accuracy for all regions and seasons.

This study does not present information as to how DMSP satellites are tested for sensor accuracy. The process to ensure sensor readings are correct (e.g. calibration) is left for others to evaluate. However, error possibilities will be presented.

Results

The study created a combined total of over 13,300 data pairs for twelve data sets: the four locations mentioned above for summer, fall and winter seasons. Overall, TS produced 7 % more data than CV. For most locations both algorithms exhibited a cold

bias: the algorithm temperature had the tendency to be colder than the actual temperature. However, CV had a warm bias for all three seasons in Saudi Arabia. CV met the accuracy criteria of ≤ 8 degrees Kelvin (K) Root Mean Square Error (RMSE) 16 % more often than TS. However, CV was on average 1.0 K RMSE more accurate than TS.

Summary

The main purpose of this research is to provide the production and accuracy characteristics of the TS and CV algorithms for AFWA. A comparison study showed how the algorithms performed in different geographic locations and at different times of the year. The algorithm outputs were compared to each other as well as to the conventional weather station surface temperatures. Overall, TS produced more output than CV, but CV was more accurate.

II. Background

Chapter Overview

After an introduction to the physics of electromagnetic radiation, this chapter provides a short history of microwave remote sensing. The satellite platform and its microwave sensor particular to this study are then discussed. Special emphasis is placed on what the sensor sees or detects. In turn, what the microwave sensor provides as output is discussed in the context of antenna theory. A radiative transfer equation describing radiation received at the satellite is then outlined in detail. Some potential solutions to such an equation are reviewed, including the solution method of choice: Statistical Inversion Method. Such a solution results in the two algorithms under scrutiny which are compared and contrasted. After discussing applications of the microwave derived surface temperatures, the chapter presents sources of error in retrieving surface temperatures from microwave measurements. Finally, the chapter ends with a current literature review of the determination of land surface temperature via remote sensing.

Introduction

The algorithms under consideration use microwave radiation sensed aboard satellites to calculate "skin" temperatures. "Skin" refers to the very top layer of the bare soil, vegetated soil, and/or snow cover. This study compares the skin temperatures to conventional weather station surface temperatures. The standard height of a thermometer at a weather station is 1.5 meters above the ground (McIlveen, 1986). For this thesis,

both skin and weather station temperature will be referred to as *surface temperature*, but conceptualized as the temperature of the air near the ground. Before describing the algorithms that calculate the land surface temperature, much background information will be covered to fully understand how the algorithms function.

Electromagnetic (EM) Radiation

All objects not at absolute zero (0 K) emit energy across a continuous range of frequencies or wavelengths. The entire range of frequencies comprises the electromagnetic spectrum (Rees, 1990).

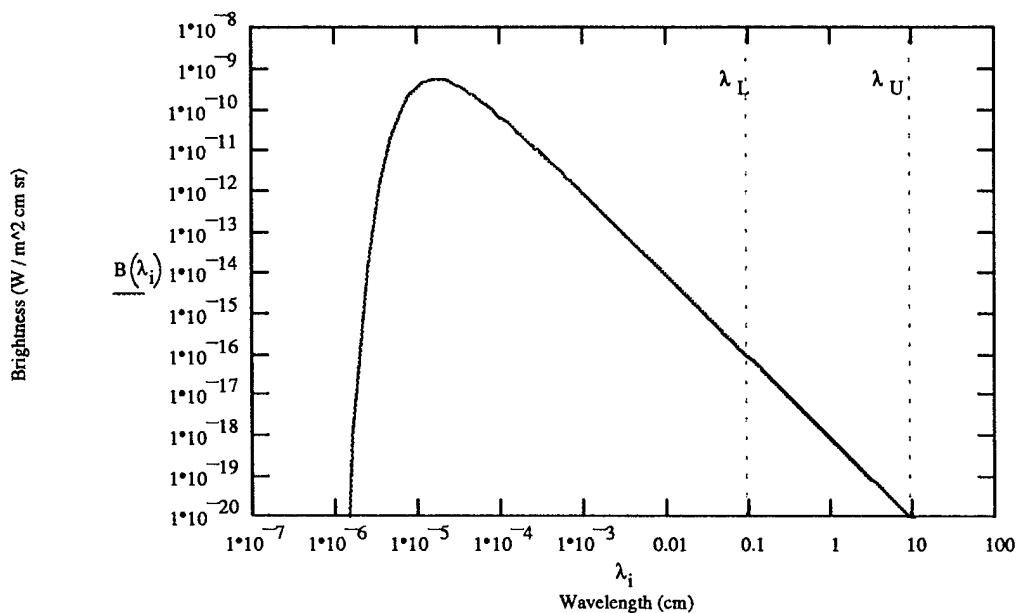


Figure 1. Wavelength Distribution of Earth ($T=300$ K) with Highlighted Microwave Region. $B(\lambda) = \text{Brightness (Watt m}^{-2} \text{ cm}^{-1})$ and $\lambda = \text{wavelength (cm)}$.

Each object has a particular distribution of wavelengths across the EM spectrum that is a function of the object's temperature. The focus here is the earth-atmosphere interface where the surface temperature is measured. The wavelength distribution for such an interface is shown in Figure 1. The figure presents the amount of the radiation emitted, termed brightness, plotted against wavelength using a mean surface temperature of 300 K.

The peak of the curve in Figure 1 shows the earth-atmosphere interface primarily transmits in the infrared portion of the electromagnetic spectrum (3 μm to 15 μm). Most weather satellite measurements observe the infrared (IR) and visible (VIS) portion of the EM spectrum, the most common being the satellite imagery used everyday in TV meteorology broadcasting. However when sensing surface temperatures from space, the IR or VIS portion of the EM spectrum is fraught with difficulties as other radiation sources interfere with the emission from the surface. Thus, scientists look to other portions of the EM spectrum. Figure 1 also shows a significant but smaller portion of the earth's emitted energy is in the microwave region (vertical markers). The microwave region is generally considered to span the range from 0.1 cm to 10 cm, or in terms of frequency, from 3 GHz to 300 GHz (Janssen, 1993).

The microwave region looked promising for several reasons. Ulaby (1981) gives four main reasons for the use of microwaves in remote sensing. First, microwaves can penetrate clouds (unlike IR). Second, microwaves are independent of sun's illumination so that the sensor can measure during the nighttime (unlike VIS but similar to IR). Third, microwaves are able to penetrate into vegetation (such as dense jungle) and even soil. Finally, microwaves are simply different from VIS and IR. Data gathered in all three

regions of the EM spectrum would complement each other and yield more information in the aggregate.

This study compares the surface temperatures observed at weather stations to satellite derived temperature readings of the same portion of the atmosphere. What follows is a contrast of the processes and instruments used for those two readings.

The standard bulb thermometer at a weather station measures the surface temperature through conduction, i.e., contact with the air. The molecular motions (kinetic energy) of the air molecules are transferred to the liquid molecules in the thermometer. In contrast, the geometric (orientation) and emission properties of the earth's surface and intervening volume (atmosphere) determine the microwave temperature readings from an earthward looking satellite (Ulaby, 1981). The latter process is radiative transfer of energy and the former process is conductive transfer of energy. For space-based observations, radiation and the effects during the radiation's propagation through the atmosphere determine the observed surface temperature. As such, thermometers are direct sensors while space observations are remote sensors. "Radiometer" is the name given to a remote sensing instrument that measures EM radiation. A radiometer is a receiver (passive system) as opposed to radars that send as well as receive EM energy (active systems). The remote sensing instrument of interest is referred to as a passive microwave radiometer and is a very sensitive receiver capable of measuring low levels of microwave radiation (Ulaby, 1981). Figure 1 shows the relatively low amounts of microwave radiation emitted from the earth-atmosphere interface.

With the goal of understanding how passive microwave radiometers detect surface radiation, the emitted radiation from the earth-atmosphere interface must be described. The flow of radiation from a source to a receiver is called radiative transfer. An equation describes the transfer process – how the radiation is affected from source to receiver. Three main effects need explanation: ground, atmosphere (medium), and radiometer (receiver). The radiative transfer equation can have many forms. The equation developed here describes microwave energy flowing from the earth and sky through the atmosphere until it reaches the satellite receiver.

Assuming the earth had no atmosphere and was a perfect absorber and emitter of radiation (referred to as a blackbody), Planck's Law describes the amount of emitted radiation. Planck's law states the surface brightness is the flow of energy across a unit area, per unit time, per unit frequency interval, from in all directions, and is given by (Ulaby, 1986):

$$B_{\nu}(T) = \frac{2h\nu^3}{c^2} \frac{1}{e^{h\nu/kT} - 1} \quad (1)$$

where B_{ν} = Surface brightness or radiance ($\text{W m}^{-2} \text{sr}^{-1} \text{Hz}^{-1}$)

ν = Frequency (Hz)

T = Physical temperature (K)

h = Planck's constant ($6.6256 \times 10^{-34} \text{ J s}$)

k = Boltzman's constant ($1.3805 \times 10^{-23} \text{ J K}^{-1}$)

c = Speed of light ($2.9979 \times 10^8 \text{ m s}^{-1}$)

Note Equation (1) is for a particular frequency. The radiometer of concern in this study uses four frequencies (more on this later).

Since the focus here is the microwave region, the Rayleigh-Jeans approximation can be used. An exponential Taylor series is applied to estimate the e^x term in Equation (1) (Spiegel, 1993 & Ulaby, 1981)

$$e^x = 1 + x + \frac{x^2}{2!} + \frac{x^3}{3!} + \dots \quad (2)$$

With $x \equiv hv/kT$ and noting for microwaves $hv/kT \ll 1$ for Earth-like temperatures, Equation (2) simplifies to $e^x = 1+x$. In turn, Equation (1) simplifies to:

$$B_\nu(T) = \frac{2\nu^2 kT}{c^2} \quad (3)$$

or alternatively since $\nu = c/\lambda$, Equation (3) can be changed to the wavelength form:

$$B_\lambda(T) = \frac{2kT}{\lambda^2} \quad (4)$$

The important outcome of the Rayleigh-Jeans approximation is the linear relationship between brightness and temperature. Figure 2 shows the linear approximation to the original Planck function is quite good for the microwave region. In fact, the Rayleigh-Jeans approximation has only a 1 % deviation from Planck's law for earth applications if $\lambda > 2.57$ mm or $\nu < 117$ GHz (Ulaby, 1981). The radiometer used in this study, called the Special Sensor Microwave Imager (SSM/I), functions within these constraints.

Non-Blackbody and Land Effects

A blackbody is an idealized material that absorbs all the incident radiation at all frequencies, reflecting none. Another aspect of a blackbody is it acts as a perfect emitter. It is assumed the blackbody is in thermodynamic equilibrium with its environment: energy is absorbed and emitted at the same rate resulting in a constant temperature.

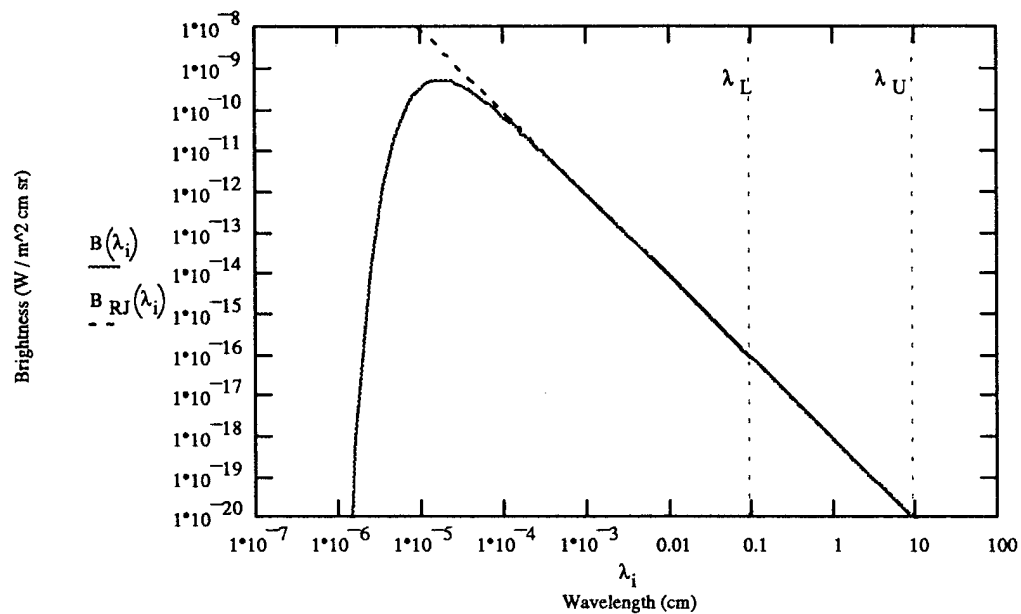


Figure 2. Rayleigh-Jeans Approximation
(B_{RJ} & dashed line on curve) to the Planck Function.

Real materials, non-blackbodies such as the earth's land surfaces and atmosphere, emit less than and do not absorb as much as a blackbody. The physical property called emissivity accounts for this departure. Emissivity, ϵ , is defined as the ratio of brightness of a non-blackbody (B) to the blackbody brightness (B_{bb}) or ratio of the brightness temperature (T_B) to the physical temperature (T) for microwave radiation (Ulaby, 1981):

$$\epsilon = \frac{B}{B_{bb}} = \frac{T_B}{T} \quad (5)$$

In other words, emissivity is a measure of a surface's ability to radiate energy and depends on the molecular structure of the surface (Conway, 1997). T_B varies from zero up to a maximum value equal to the physical temperature of the scene. Representing radiation from a scene, T_B is the end product of a radiometer measurement. However, T , the physical temperature, is the goal of algorithms in this study. Exactly how the physical temperature is retrieved from the brightness temperature will be explained in later sections. Equation (5) assumes the material is homogeneous and of uniform temperature. Both assumptions may be an oversimplification for sensing temperatures near the ground. In contrast, the assumption of homogeneity is more valid for an ocean surface. As McFarland (1991) points out, land emissivities are more variable both in space and time. Spatial variances arise from vegetation, topography, urban features, bodies of water, etc. Examples of temporal changes are caused by vegetation changes both natural and artificial (agricultural), soil moisture changes, and snow cover morphology. For both land and ocean surfaces, another emissivity complication is surface roughness, which generally reduces the radiance sensed by the radiometer by diffusion (Ulaby, 1993).

Another surface property at the earth-atmosphere interface is reflectivity, r . Some energy reaching the radiometer is due to reflection. Reflectivity is closely related to emissivity. Assuming no transmission through the body, non-blackbodies reflect the incident energy if it is not absorbed, as shown by Equation (6).

$$1 = \epsilon + r \quad (6)$$

Reflectivity at a surface is also referred to as surface scattering. The equation for emissivity (Eq. 5) implies if the brightness temperature measured by the satellite radiometer and the surface emissivity are known then the physical temperature of the scene can be determined assuming no atmospheric influence on the radiation as it propagates between surface and receiver. This is one approach in determining surface temperatures from space. Unfortunately, several complexities arise which are explained in later sections. Another aspect of EM radiation is polarization.

Electromagnetic radiation travels in waves. As the name implies, two fields define radiation: electric and magnetic. A combined wave simultaneously represents each of these fields. These two waves are always perpendicular to each other and to the direction of propagation. Polarization is the orientation of these fields (Rees, 1990) with respect to a coordinate system. For example, a sensor could be sensitive to the vertical or horizontal orientation of the EM wave.

With the basic EM knowledge and terminology known, the next section, paraphrased from Ulaby (1981), provides a context of the present state of passive satellite microwave radiometry (PMR).

Remote Sensing History

Using frequencies near the microwave portion of the EM spectrum, the first remote sensing experiment occurred more than 110 years ago in 1886. In the 1920's, the Naval Research Lab (NRL) pioneered the use of radars to detect ships, aircraft, and the height of

the ionosphere. The NRL is mentioned because they served as technical consultant to the Department of Defense's (DoD) atmospheric remote sensing system under investigation in this paper. Airborne detection systems using microwaves became a reality in the early 1940's. As opposed to the active systems just mentioned, PMR first developed in the 1930's and 1940's to measure radiation from space. Terrestrial microwave radiometry (looking down) had its beginning in the late 1950's. Synthetic aperture radar began in the 1950's. This was a major improvement in resolution that paved the way for space-borne imaging radars (Ulaby, 1981).

NASA deployed its first space-borne passive microwave radiometer over Venus with the Mariner 2 spacecraft in December 1962. The USSR flew the first earth-viewing atmospheric passive microwave radiometer in 1968 aboard the Cosmos 243 satellite. The US National Oceanographic and Atmospheric Administration (NOAA) followed in 1972 with an atmospheric passive microwave radiometer aboard the Nimbus 5 satellite. The US Defense Meteorological Satellite Program (DMSP) deployed its first atmospheric passive microwave radiometer in 1978 to sense atmospheric profiles of temperature (Ulaby, 1981). The Special Sensor Microwave Imager (SSM/I) instrument on board the DMSP satellite F8 was first sent aloft in 1987, a full 25 years after Mariner 2's pioneering journey (Hesser, 1995).

Atmospheric PMR has concentrated on soundings and ocean parameters such as wind speed over water and sea ice. Researchers investigated some land parameters such as soil moisture, but surface temperature has been neglected in microwave remote sensing (McFarland, 1991). Surface temperatures are important to all the military services for the

following reasons. First, most atmospheric numerical models use global surface temperature as a key input. Second, near real time surface temperatures over enemy held or data-sparse areas are needed for target weather analysis and forecasts.

The pioneering instruments mentioned above were rather simple sensors using few channels with limited resolution. As of this writing, the DMSP SSM/I still represents some of the most advanced technology in space-borne PMR. Only DMSP SSM/I data were used in this study. The next section details information about this system.

DMSP and the SSMI

First launched in 1970, DMSP Block V satellites represented state of the art technology with such advancements as 0.62 km visual imagery resolution – the highest resolution of any weather satellite then and even today almost 30 years later (Fett et al, 1997). Currently operational, DMSP satellites F13 and F14 are in a near circular polar orbit at a mean altitude of 850 km. The spacecraft is about the size of an average car (3.7 m long by 1.2 m high) and has a design life span of two years. The satellite makes one orbit in 102 minutes (Deuel, 1996).

Figure 3 shows both the ascending and descending paths of the SSM/I swaths over a 24 hour period (Janssen, 1993). The swath width is 1394 km. Note the data gaps in the lower latitudes. The SSM/I is a seven channel, four frequency, linearly polarized, passive microwave radiometer. The seven channels are sensitive to vertically and horizontally polarized radiation at channel-center frequencies of 19.3 GHz, 22.2 GHz, 37 GHz, and

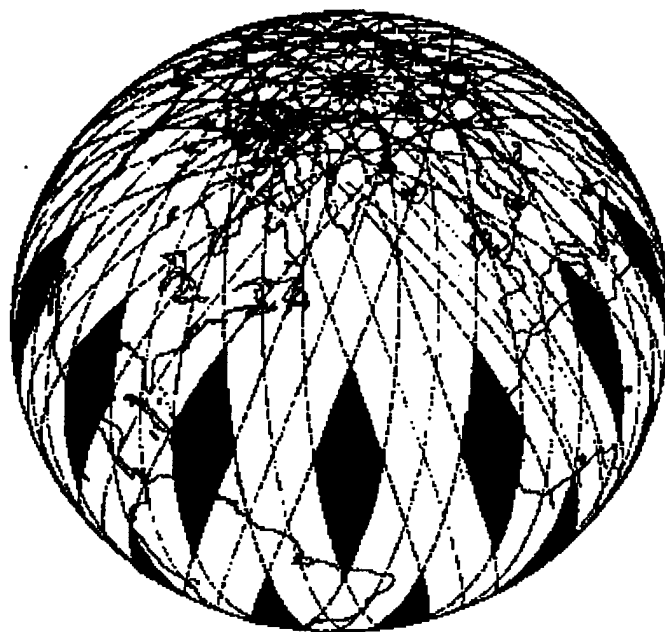


Figure 3. SSM/I Global Coverage

85.5 GHz frequencies, excluding the horizontal polarization at 22.2 GHz. The sensor measures land, atmospheric, and ocean surface brightness temperatures. In general, *imager* radiometers use frequencies in the atmospheric windows to monitor surface features such as the ones just mentioned. In contrast, *sounder* radiometers use frequencies in the less transparent portion of the EM spectrum to capture profiles of atmospheric parameters.

The four frequencies of the SSM/I are indicated with an “S” in Figure 4. The corresponding wavelengths for 19.3 GHz, 22.2 GHz, 37 GHz, and 85.5 GHz are 1.55 cm, 1.35 cm, 0.81 cm, and 0.35 cm, respectively. Figure 4 highlights the sampling intent of the SSM/I. The 19.3 GHz channel was chosen to sample the lowest layers of the atmosphere as the atmosphere is quite transparent at that frequency. The 22.2 GHz

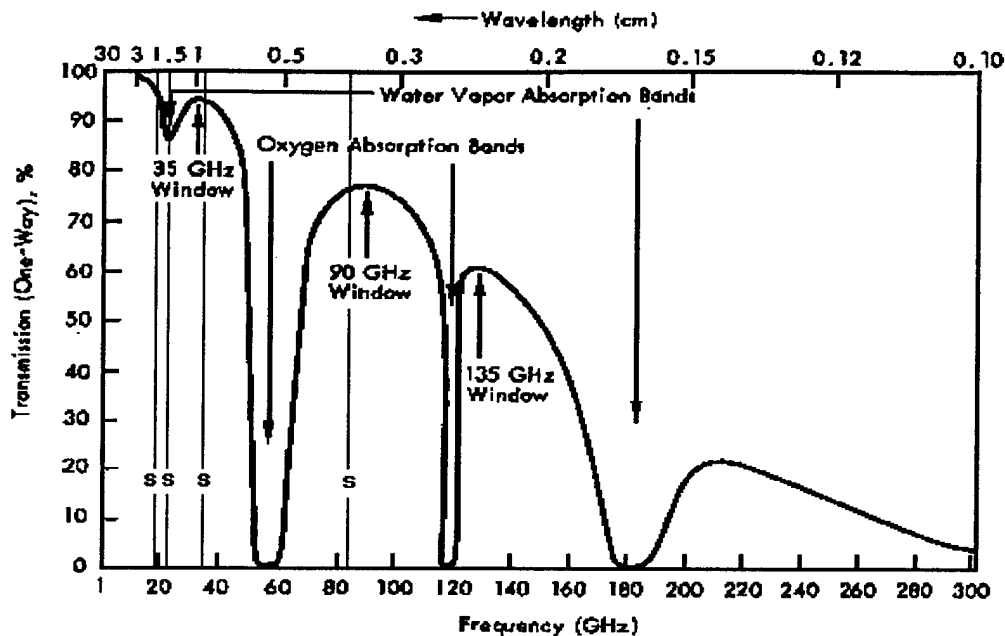


Figure 4. Percentage Transmission Through Clear Atmosphere in Vertical Direction with SSM/I Frequencies (S) (adapted from Ulaby, 1986)

frequency takes advantage of a water vapor absorption band. The 37 and 85.5 GHz frequencies were chosen to take advantage of their respective windows. However, the addition of the 85 GHz channel is a unique advancement over previous microwave imagers. With its high sensitivity, the 85 GHz channel is primarily used for measuring rainfall (Janssen, 1993).

Located on top of the satellite (see Figure 5), the instrument consists of a 45° tilted parabolic reflector (24×26 inches) which receives the scene radiation and feeds it into a broadband, seven port horn antenna which then feeds into the radiometer. This whole assembly is oriented normal to the earth's surface. Due to the curvature of the earth's

scan. Macelloni et al (1994) states the ground resolution of the 19.3 GHz, 22.2 GHz, 37 GHz, and 85.5 GHz frequencies are 43, 40, 29, and 13 km respectively. These resolutions also represent pixel sizes. The 13 km resolution of the 85 GHz channel has one of the highest resolutions ever for a microwave radiometer (Janssen, 1993). Although the frequencies were chosen for the determination of various atmospheric parameters, all four frequencies are used in the surface temperature algorithms.

The basic functions of the SSM/I instrument have been reviewed. The next section explains what the SSM/I actually senses in the context of atmospheric effects and the resulting radiative transfer equation.

Atmospheric Effects

What the instrument detects is a complex combination of several radiation sources and radiation-matter interactions. A radiometer looking at the earth senses a brightness, the origins of which are diverse. Shown in Figure 6, the energy incident on the sensor is primarily from four sources: Land emissions (1), land reflections of downward atmospheric emissions (2), land reflections of downward cosmic emissions (3), and upward atmospheric emissions (4) (Ulaby, 1981).

With Figure 6 in mind, the scene that the radiometer views is actually a cylinder pointed in a particular direction. The direction is quantified by an azimuth angle (ϕ) and elevation angle (θ). Sources (1) and (3) are relatively simple to account for in that the atmosphere reduces the radiation along the way to the radiometer. Sources (2) and (4), atmospheric emissions, are more complex because each layer in the atmosphere emits

radiation which is simultaneously reduced by absorption before it reaches the receiver. Before these sources and effects are examined, some general radiative transfer process must be described.

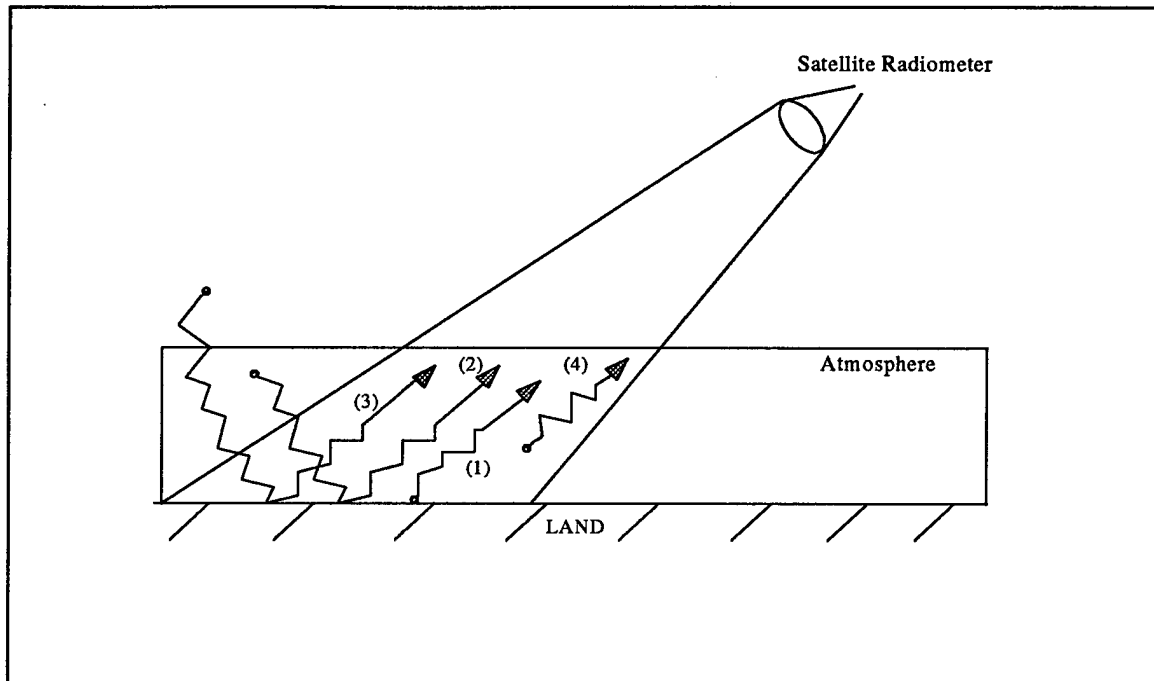


Figure 6. Satellite Radiometer Sources of Radiation.

There are two processes that occur between radiation and the medium (in this case the atmosphere) in which the radiation propagates: emission and extinction.

Extinction of radiation by the medium involves the two effects of scattering and absorption. Scattering here refers to radiation diverted out of the radiometer's path. In contrast, emission scattering means scattering into the radiometer's view path. Absorption means the radiation is transformed to other forms of energy, such as heat (Ulaby, 1981). The effect of extinction can be expressed in the term κ_e (extinction coefficient). Like

emissivity, κ_e is a value between 0 and 1. Because it depends on the distance traveled in the medium, extinction can be combined with distance, z , to form a single factor which is called optical depth, τ where

$$\tau(z, \infty) = \int_z^{\infty} \kappa(z) dz \quad (7)$$

Note from Figure 6, the entire atmosphere affects all the radiation sources from the surface (0) to the top of the atmosphere (H). The optical depth is sometimes referred to as opacity – extent to which a given layer of material reduces the intensity of the radiation (Rees, 1990). The atmosphere reduces in density and hence extinction with height. The non-linear decrease of extinction can be expressed with an exponential function as $e^{-\tau(z, \infty)}$. This reduction factor must be applied to all sources of upwelling radiation.

The surface emission (emissivity), introduced with Equation (5), needs expanding to explain medium or volume emission. Two sources of radiation affect volume emission. Note, thermodynamic equilibrium is assumed, thereby emission equals absorption. The first emission source is the radiation emitted by the matter. The second source to enhance emission is scattering of radiation into the direction of the radiometer from other matter outside of the cylinder viewed by the radiometer – emission scattering. Like opacity, the upwelling radiation emitted by the atmosphere decreases with height. In contrast to the single radiation sources at the surface, a sum (integral) of sources from many layers is used to describe the atmospheric emission. The atmosphere's emission contribution can be expressed using the product of κ_e and its brightness for each increment of height, dz .

However, just like the earth's emission, the atmosphere's emission at each layer is also reduced by extinction on its way up to the radiometer. Thus, the reduction factor, $e^{-\tau(z,\infty)}$, is also applied to the atmospheric source term as it was to the surface radiation sources. In essence, the reduction factor is applied twice. However for microwave radiometry, the scattering contribution to extinction can be ignored. As Janssen (1993) states, the common remote sensing frequency range from about 20 GHz to 90 GHz contains certain frequencies where absorption due to liquid clouds is at least two orders of magnitude greater than the scattering. If scattering is neglected error rates are less than 1%.

By using Hollinger (1983) and Ulaby (1986) as a guide, the above effects are applied to the radiation sources in a radiative transfer equation. Using Equation (4), the Rayleigh-Jeans Law, brightness temperatures represent the surface and atmosphere source radiances. The equation must also include the effects of emissivity and reflectivity. The resulting equation is rather complex.

$$T_{AP}(H) = \epsilon T_G e^{-\tau} + r T_{sky} e^{-2\tau} + \int_0^H \kappa_e T_{A-up} e^{-\tau} dz + r \left[\int_0^H \kappa_e T_{A-down} e^{-\tau} dz \right] e^{-\tau} \quad (8)$$

where T_{AP} = Apparent brightness temperature at satellite height H (K)

ϵ = Emissivity of ground

T_G = Physical temperature of ground (K)

$e^{-\tau}$ = Atmospheric reduction factor (transmissivity of entire atmosphere)

τ = Optical depth above level z

r = Reflectivity by the ground

T_{sky} = Brightness temperature of cosmic and galactic sources

κ_e = Atmospheric extinction coefficient

T_{A-down} & T_{A-up} = Physical temperature of infinitesimally small atmospheric layer

Equation (8) represents what the radiometer sees – radiation from the four sources in Figure 6. The first term is the surface-emission blackbody brightness temperature (equal to the physical temperature) reduced by its emissivity (non-blackbody characteristic) and the intervening atmosphere's transmission (or transmissivity). The second term is the cosmic and galactic background radiation reduced three times: atmospheric extinction inbound to the earth, reflection off the earth, and then atmospheric extinction again outbound to the satellite. The third term represents upward atmospheric emission. The product, $\kappa_a T_{A-up} dz$, is the brightness contribution from a thin atmospheric layer that is reduced on the way up to the radiometer by the atmospheric absorption factor, $e^{-\tau}$. The integration sums the brightness contributions for all atmospheric layers. The last term represents downward atmospheric emissions reduced similarly to T_{sky} . Note all the optical path terms are implicitly multiplied by $\sec \theta$, which is the slant path up to the radiometer. Equation (8) has many unknowns and the intent of showing the reader this equation is to demonstrate the many complexities of describing the radiation viewed by a satellite.

The radiative transfer equation illustrated by Equation (8) shows if all the variables on the right-hand side of the equation are known, then the brightness temperature measured at the satellite can be calculated. This is an example of a forward problem. In reality, the situation is an inverse problem. The satellite provides the brightness temperature and the unknowns on the right hand side of Equation (8) must be determined in order to solve for the surface temperature (Janssen, 1993). As Ulaby (1986) points out, such an inverse problem does not have a straightforward solution.

The treatment of the unknowns will be presented in a later section describing the SSM/I surface temperature retrieval technique. Until then, exactly what the satellite provides as output must be explained. Table 1 shows some typical brightness temperatures for one SSM/I frequency received from the Air Force Weather Agency (AFWA).

In reality the satellite does not observe, or provide as an output, brightness temperatures. The next section briefly outlines the principles of taking radiometric measurements and how the brightness temperatures in Table 1 were derived.

Table 1 - Brightness Temperatures for the 19 GHz SSM/I Frequency

Brightness Temp. (K)	I-Coord.	J-Coord.	K-Coord.
134.0	1	1	43
135.0	2	1	43
136.0	3	1	43

Antenna Theory

The function of a radiometer is to measure brightness (or radiant intensity). The brightness is an idealized flow of power in infinitesimally small elements of bandwidth (Janssen, 1993). The passive antenna can be defined as a region of transition between a propagating electromagnetic wave in space and a guided wave propagating in a

transmission line (voltage in a wire) (Ulaby, 1981). Antennas are usually made of metal so as to conduct electron voltages. The electromagnetic wave induces a fluctuating current in the antenna. This current or power, P, is represented by

$$P = T_{AP} A_f F_n k \Delta v \quad (9)$$

where T_{AP} = Apparent brightness temperature
 A_f = Antenna physical receiving area
 F_n = Antenna electromagnetic pattern
 k = Boltzmann's constant
 Δv = Bandwidth

As in Equation (8), T_{AP} is the apparent brightness temperature measured by the satellite radiometer. A_f , F_n , and Δv are known from the engineering of the antenna. The power or voltage counts for each of the SSM/I frequencies is the actual output of the radiometer. These voltage counts are transmitted to various sites on the earth. Using the voltage counts, and solving for T_{AP} in an equation like Equation (9), the P values are converted to brightness temperatures (as in Table 1) at AFWA, Offutt AFB.

The brightness temperatures are then mapped onto a polar stereographic grid (Figure 7) which is 512×512 grid points in dimension for a hemisphere. Each box has a grid dimension of 64×64 . Note there are two grid-referencing systems for Figure 7. First, a point on the globe can be represented by the I, J, K coordinates. For example, a point in the western CONUS might be 1, 39, 44. The 44 coordinate corresponds to the box over the central US and Canada as shown in Figure 7. A point could also be represented with just two coordinates, I and J, using the fact the whole hemisphere has dimension 512×512 . Thus, the same point mentioned above in the 44 box would be 193, 359. The

brightness temperatures mapped onto the grid are referred to as the Sensor Data Record (SDR) and were used in this study as input to the surface temperature algorithms.

It has been shown what the radiometer measures, what the radiometer provides as output, and how this output is converted to a brightness temperature. The last question to answer is how to solve the inverse problem, i.e., how to obtain surface temperatures from the brightness temperatures.

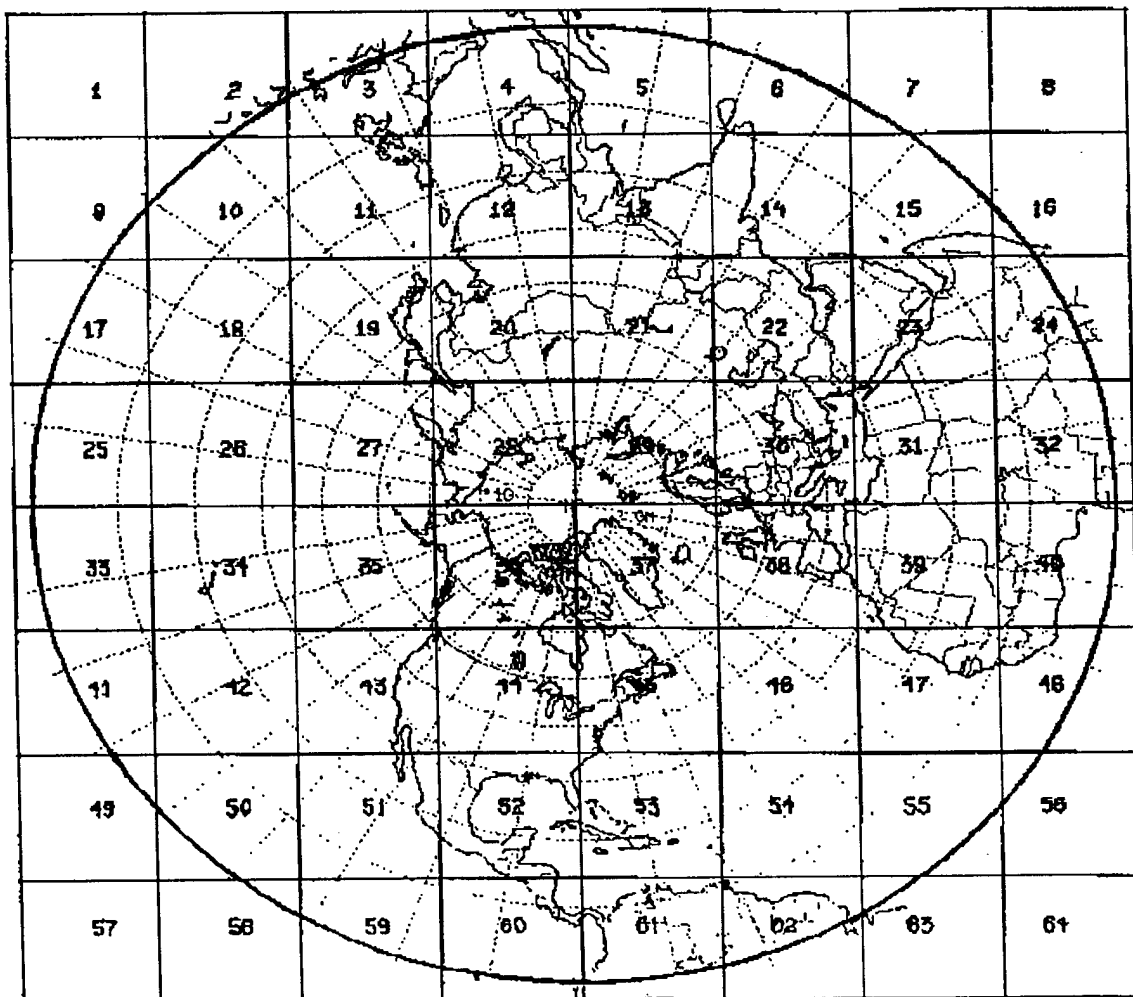


Figure 7. Polar Stereographic Northern Hemisphere Grid

Temperature Retrieval Technique – Statistical Inversion Method

The goal is to find a function that relates values of $T_{AP}(v)$ (the measured brightness temperatures for various frequencies) to the surface temperature for various land types. The function can be written in a manner similar to Equation (8) where the brightness temperatures are written on the right-hand side and the surface temperatures on the right. Writing both sets of temperatures in vector form yields:

$$T_{AP} = W T \quad (10)$$

where T_{AP} = radiometric observations for various frequencies from a particular land type
 W = weighting matrix
 T = surface temperatures for a particular land type

T_{AP} has dimension or order n corresponding to the number of microwave frequencies, T has order m corresponding to the number of surface temperatures taken for a particular land types, and W is of dimension $m \times n$. Equation (10) is a simple representation of the complex radiative transfer process in Equation (8) in which the brightness temperatures derived from the satellite are a function of the physical temperature. The relation or weighting matrix represents all the other radiation-matter interaction terms in Equation (8). Equation (10) assumes a linear relationship and Gaussian distribution of temperatures (Ulaby, 1996). The Raleigh-Jeans approximation validates the linear assumption. The fact that atmospheric parameters follow a Gaussian distribution when the sample size is large enough to evoke the central limit theorem validates the Gaussian assumption (Wilks, 1993). Solving for the desired surface temperatures gives Equation (11).

$$\mathbf{T} = \mathbf{W}^{-1} \mathbf{T}_{AP} \quad (11)$$

There are many inversion techniques that provide the relation matrix, \mathbf{W}^{-1} (Ulaby, 1986). The SSM/I program uses the statistical inversion method (SIM) (Hollinger, 1983). SIM essentially determines \mathbf{W}^{-1} with multiple-linear regression. Empirically, several sets of radiometric measurements for various microwave frequencies (\mathbf{T}_{AP}) is obtained corresponding to simultaneous measurements of \mathbf{T} (surface temperatures). The study obtains several sets of brightness and surface temperatures, each set corresponding to a different land type. Standard regression programs are then used to derive the relation matrix. Hollinger (1983) used a very similar equation to Equation (11) for application to the SSM/I,

$$\mathbf{P} = \mathbf{D} \mathbf{t} \quad (12)$$

where \mathbf{P} = vector of surface temperature estimates
 \mathbf{t} = vector of brightness temperatures
 \mathbf{D} = correlation coefficient matrix which relates \mathbf{P} & \mathbf{t}

Note there is no actual inversion of any matrix when determining the brightness-physical temperature relationship. "Inversion" means the overall problem is a backward one in terms of standard radiative-transfer equations – solving for the right-hand side versus the left-hand side of the equation. Multiple-linear regression is used to define the relationship between brightness temperatures and physical temperatures. The regression coefficients and frequency variables are then put in algorithm form (as shown in the next chapter). The result is a set of algorithms where each algorithm is used for a particular

land type. Operationally, the real time brightness temperature measurements (t) serve as input to the algorithms.

Janssen (1993) adds an error term ($\epsilon = \epsilon_1 + \epsilon_2 + \epsilon_3 \dots$) to equation (12). The errors could be caused by several reasons inherent to remote sensing: radiometer noise, linearization, unknown parameters, and weighting functions. The end of this chapter contains a full discussion of errors.

With the generation of the algorithm set complete, where each algorithm pertains to a particular land type, the land type must be known to retrieve a surface temperature. An empirical approach is used to determine the land type relationship. The power or brightness temperature from each channel usually falls within a certain range. These ranges are experimentally determined for various land types and then combinations of these ranges are put in rule form. For example, the land type dry arable soil is determined in the CV algorithm with the following rule:

If $(V22 - V19) \leq 4.0$ and
 $4.0 < (V19 + V37)/2 \leq 9.8$ and
 $(V37 - V19) \geq -6.5$ and
 $-5.0 \leq (V85 - V37) < 0.5$ and
 $(V85 - H37) < 4.2$ then
land type = dry arable soil

where V22 = Vertically polarized 22.2 GHz
V19 = Vertically polarized 19.3 GHz
V85 = Vertically polarized 85.5 GHz
V37 = Vertically polarized 37.0 GHz
H37 = Horizontally polarized 37.0 GHz

With similar rules established for the various land types, the rules are applied to the SSM/I channel measurements to determine the land type. With the land type determined,

the corresponding surface temperature algorithm is used to calculate the surface temperature. The land type rules are not all inclusive. Some channel measurements do not fall into one of the land type rules and thus a land type, and in turn, a surface temperature is undeterminable. As a result, the land typing schemes affect the quantity of algorithm-produced surface temperatures.

In summary, the method used with SSM/I data to calculate surface temperatures does not require prior (a priori) knowledge of the unknowns in Equation (8): temperature profiles, emissivity, reflectivity, absorption, scattering, etc. of the earth-atmosphere system. Instead, what is needed is a priori knowledge of the relation between measured brightness temperature at seven channels and measured physical temperature for various land types. Multiple linear regression determines those relationships. The regression coefficients are used to build sets of TS and CV surface temperature algorithms, each algorithm corresponding to a particular land type. A priori knowledge of the land typing schemes is required to choose which algorithm to use in the set.

Calibration/Validation (CV) Algorithm and FORTRAN Code

Still in wide use, the CV algorithm in this study is based upon the land surface temperature algorithm as outlined by McFarland (1991). The Naval Research Laboratory (NRL) produced CV in 1988 to calibrate and validate the SSM/I. The algorithm is a linear combination of coefficients applied to the SSM/I frequencies, but only 4 channels are used: 19H, 22V, 37V, and 85V. Different algorithms are used based upon one of four different land types classifications as shown in Table 2.

The CV program was quite concise – only four pages of code. The program consisted of two main routines. First, the land type was determined using eight land type rules, as shown previously for dry arable soil. The similar land type classifications (e.g. moist soils) were combined into the four general land type classifications listed in Table 2. Second, based upon one of the four general land types, the corresponding algorithm from Table 2 was run to obtain the surface temperature. As mentioned, the land type classifications and/or rules were not all inclusive. Occasionally, the program could not determine a land type, and in turn a surface temperature could not be calculated.

Moncet et al (1996) states the major advantages of the relatively simple statistical inversion method for the SSM/I derived parameters are robustness and operational expediency. The CV code is certainly expedient. However, he points out the dependence on a linear relationship and lack of a non-linear treatment of the background conditions

Table 2. CV Land Surface Temperature Algorithms

LAND TYPE	ALGORITHM
Dense Vegetation	$T(K) = 24.94 - 1.2784(T19H) + .88(T22V) + .5933(T37V) + .7299(T85V)$
Agricultural/Range	$T(K) = 6.97 - .6266(T19H) + .2716(T22V) - .1297(T37V) + 1.482(T85V)$
Moist Soils	$T(K) = 23.16 - .1873(T19H) + .5221(T22V) - .6271(T37V) + 1.232(T85V)$
Dry Soils	$T(K) = 72.68 - .4598(T19H) + .5984(T22V) + .8828(T37V) - .2623(T85V)$

(e.g. emissivity, reflectivity) may lead to a large spread of retrieval errors (see error discussion at end of chapter). McFarland (1991) points out the downside of this technique for retrieving land surface temperatures as the simple treatment of the land types. Land surfaces not only vary a great deal spatially, but also temporally. Temporal variances occur throughout the year and from year to year both from natural and man-made changes in the land surface.

Temperature from Sensor Microwave Imager (TS) Algorithm and FORTRAN Code

In contrast to the CV algorithm, the TS algorithm uses all seven channels to obtain a surface temperature (See Table 3 below). Additionally, TS applies eight land types with the potential for a total of 25 different land surfaces. Currently, the snow and ice background land types are turned off due to unreliability (Kopp, 1997). Note the TS algorithms incorporate the viewing angle (θ) as well. Another difference between CV and TS is AFWA calculates new TS coefficients for each new DMSP satellite. Theoretically each new satellite and its SSM/I has a slightly different viewing angle from the previous satellite and thus, the relation between brightness temperature and physical temperature should change as well. CV coefficients and their algorithms have been constant since their inception in 1987.

Three times the length of CV, the TS program (15 pages) is significantly more complex than the CV program. However, the TS code is tunable which allows for continuous improvement over time. CV is not tunable.

Table 3. TS Land Surface Temperature Algorithms for DMSP F13 (provided by AFWA)

LAND TYPE	ALGORITHM
Densely & Moderately Vegetated Land, Cold Vegetated Land	$T(K) = 18.833 + .8557(T22V) - .23(T37V) + .9349(T85V) - .6188(T85H) + .4235(\theta)$
Arable Soil	$T(K) = 29.926 - 1.087(T19H) + 3.276(T22V) - 1.664(T37H) + 10.357(T85H) - 1.829(T85V) + 5.243(\theta)$
Snow & Deep Snow Covered Land	Not Used
Glacial Snow	Not Used
Morning Desert	$T(K) = 133.173 + 2.07(T19H) + 7.464(T22V) - 9.741(T37V) + 2.016(T37H) + 6.967(T85V) - 3.155(T85H) + 5.324(\theta)$
Sparsely Vegetated Land	$T(K) = 73.304 + 7.456(T22V) - 7.546(T37V) + 2.557(T35H) + 9.275(T85V) - 3.993(T85H) + 1.431(\theta)$
Flooded Land	$T(K) = -4.301 - 2.554(T19H) + 12.837(T22V) - 8.893(T37V) + 2.889(T37H) + 14.717(T85V) - 8.805(T85H) + 4.555(\theta)$
Desert, Wet Surface	$T(K) = 109.079 - 7.194(T19V) + .2841(T19H) + .6520(T22V) - 2.919(T37V) + 14.223(T85V) - .6845(T85H)$

Applications of SSM/I Data

This paper addresses two applications of the algorithms in question, both of which are currently operational at the AF Weather Agency (AFWA). The TS algorithm is primarily used in two capacities. First, TS serves as one input for the global surface temperature model, Surface Temperature (SFCTMP). Secondly, TS aids the analysis of global cloud coverage (Kopp, 1995). Existing as a sub-set of a cloud model called Real-Time Nephanalysis (RTNEPH), TS was rewritten in 1990 as part of an overall improvement effort to analyze and forecast clouds (Kopp, 1995). To analyze clouds in data sparse areas, AFWA uses the TS output to first determine if clouds are present by comparing the IR temperature to the background surface temperature partly derived from SSM/I data. If the IR temperature is colder than the surface temperature then a cloud is assumed to be present (Kopp, 1994). If the derived background temperature is the same as the IR temperature, when in fact the real background surface temperature is warmer than the IR temperature, the analysis will falsely show no cloud present.

The second application addressed here is the desire of military forecasters to have near real-time surface temperatures from data sparse or denied territory. Among many applications, surface temperature is a key element in the ability of precision guided munitions to acquire their targets. Heavily based upon the temperature, forecasters will brief if there is enough thermal contrast between the target and it's background. To assist in the determination of surface temperatures, the USAF is currently fielding its newest deployable satellite imagery receiver called the Small Tactical Terminal (STT). The STT uses the CV algorithm to create the surface temperature products (Harris Corp., 1997).

Deployed forecasters need to know the average departures from truth (bias) and accuracy of the surface temperatures produced by CV.

Sources of Error

According to Janssen (1993), radiometric errors can arise from essentially four sources: radiometer noise, linearization, unknown parameters, and regression.

The first is radiometer noise, which is composed of random and bias components. Random noise is Gaussian in nature and thus has known statistics. However, bias is not obvious and must be reduced to tolerable levels by calibration and comparison of the derived products with ground truth data. Bias will be uncovered in this study. AFWA regularly calculates and removes the bias.

Second, linearization errors may occur due to the Raleigh-Jeans approximation. If these errors are not less than the radiometer noise then other inversion methods must be applied.

Third, errors from unknown parameters exist. For example, the land typing is not exact due to the high spatial and temporal variability of land types. Another example of errors from unknown parameters is changes in satellite viewing angle. Fuhrhop and Simmer (1995) performed a study on SSM/I radiometers and found the variations of viewing angle to be as high as 1.5 degrees which results in a brightness temperature change of 2 K. By analyzing the brightness temperature variations with changing incidence angle, a correction can be derived and used. TS corrects for variable viewing angle by including it in the regression. A third example of unknown parameters error is

the effect of hydrometers – specifically cloud water droplets and rain. As Ulaby (1981) points out, water clouds reduce microwave transmission below wavelengths of 2 cm, thus affecting all the channels on the SSM/I (wavelengths given below Figure 6). Ice clouds have almost no effect. A major source of error is rain. The rain attenuation is appreciable at wavelengths below 2 cm. However the amount of intense rain actually covering the earth to affect SSMI readings is quite small (Ulaby, 1981). Janssen (1993) points out taking measurements at other frequencies reduce the errors from unknown parameters.

Finally, there are potential errors in calculation of the regression coefficients. The multiple linear regression is only an approximation to the brightness temperature-physical temperature relationship. The regression analysis has some associated error.

Remote Sensing of Land Surface Temperatures – Literature Review

The science of Passive Microwave Radiometry (PMR) has not focused on the retrieval of surface temperatures over land in contrast to ocean parameters and atmospheric profiles. Indeed, there is no hard DoD requirement for the performance of the SSM/I derived surface temperatures (Glackin and Gasster, 1994). However, within the last several years there have been some related studies.

Over the continent of Australia, Prata (1994) investigated PMR retrieval of land surface temperatures, but his study used data from NOAA's Advanced Very High Resolution Radiometer (AVHRR). The AVHRR uses the IR portion of the EM spectrum, not the microwave portion. Also using IR, but from radiometers onboard aircraft, Chen and Engman (1997) studied the spatial pattern of moisture and temperature over the

central US prairie. They show their algorithms to generally overestimate the surface temperature by 2.5 degrees with an RMSE of 3.51 K. A study by Macelloni et al (1994) used SSM/I data to determine land types but not surface temperatures in several test areas around the globe. The original SSM/I calibration and validation (1987) of the land surface temperature algorithm is the study most similar to this thesis. Although using DMSP satellite F8 and covering only over the Western Desert and Central Plains of the US, the Naval Research Lab collected a total of 1764 data pairs for 4 days in Aug 1987. The CV algorithm performed with an RMSE of 3.1 K for all land types (McFarland, 1991). Thus, the initial work by Comoglio (1997) and continued work by this author appear to be unique.

Summary

For a given frequency, radiative transfer theory shows the physical temperature is related to brightness, and that relationship is linear for the microwave portion of the EM spectrum at Earth temperatures. For sensing land surface temperatures from space, the brightness-physical temperature relationship is complex when specifying all the sources and radiation-matter effects.

The SSM/I project overcomes this complex relationship empirically. Multiple linear regression applied to field measurements determines the temperature-brightness relationship in a set of algorithms for various land types. Operational microwave brightnesses serve as input to the algorithms, which then provide the surface temperatures. The question remains as to the performance level of the TS and CV algorithms.

III. Methodology

Chapter Overview

The methodology section explains the processing of the data and the statistics gathered from the data. The main goal of data processing was to obtain data pairs – ground station and algorithm temperature at the same time and place. Notwithstanding inherent errors, ground station data was assumed to be "truth" data.

The following chapter starts with how the current work fits in with prior AFIT research. Data sources are then described followed by a detailed explanation of the data comparison process that generates data pairs. The chapter ends with a discussion of algorithm performance statistics.

Building on Past Work at AFIT

Comoglio's (1997) work was essentially a preliminary study of algorithm performance because most of his work entailed the proper setup and execution of the algorithms on AFIT workstations. Time was not available to accomplish an extensive comparison over time and space. The task of porting the algorithms to AFIT hardware alone was considerable, especially for the TS algorithm. Since the present work was a continuation of Comoglio's research, it was imperative to precisely follow his procedures to properly combine the results.

To prove continuity of Comoglio's work, the CONUS summer 96 data set was chosen to be a trial run of the process. Table 4 displays both the Comoglio and current study's CONUS Aug 96 results. The process was duplicated well.

This study accomplished major improvements in processing and data organization. Instead of manually entering each hour of a day, programs were made to automatically cycle through all 24 hours. In addition, automation was applied to the SSM/I data files. Before each file pertaining to a particular frequency was processed separately. During the current study, all SSM/I files for one day were automatically processed together.

Data Sources and Description

The SSM/I data for the Northern Hemisphere was recorded on 8mm tapes at AFWA, Models Branch, Offutt AFB Nebraska and sent to AFIT. AFWA provided the data in UNIX gridded format as described in Chapter 2.

The SSM/I data set was organized by day. Each day had 3 file types comprising a total of 9 files per day: grid date time stamp; brightness temperatures - 7 files, one for each channel; and satellite identifier. See Table 5.

Table 4 - Comparison of Comoglio and Harris results for CONUS Aug 96.
Mean, Standard Deviation (SD) have Kelvin units (K). Variance units are K².

	Station Temperature			TS			CV		
	Harris	Comoglio	Difference	Harris	Comoglio	Difference	Harris	Comoglio	Difference
N	1377	1382	5	1098	1108	10	1072	1077	5
MISSING				279	274	5	305	305	0
MEAN	299.7	299.7	0.0	293.3	293.4	0.1	293.9	293.9	0.0
SD	6.7	6.6	0.0	7.8	7.8	0.0	5.0	5.0	0.0
VARIANCE	44.9	44.7	0.2	61.7	62.1	0.4	25.3	25.2	0.0

Table 5. SSM/I Raw Data Files

FILE TYPE	FILE NAME
Grid Date Time Stamp	RNXMI1_00MITT
19 GHz - Vertical	RNXMI1_00MIH1
19 GHz - Horizontal	RNXMI1_00MIV1
22 GHz - Vertical	RNXMI1_00MIV2
37 GHz - Horizontal	RNXMI1_00MIH3
37 GHz - Vertical	RNXMI1_00MIV3
85 GHz - Horizontal	RNXMI1_00MIH4
85 GHz - Vertical	RNXMI1_00MIV4
Satellite Identifier	RNXMI1_00MIID

The AF Combat Climatology Center (AFCCC), Asheville, North Carolina provided the ground station data in DOS format as shown in Table 6.

Table 6. Ground Station Data Formats

	---block #--- ---Date----- time-- temp K-
Raw	6901901996080100003042
Decoded	690190, 1 Aug 96, 00 hr, 00 min, 304.2 K

The block # refers to the World Meteorological Organization's geographic reference system. AFCCC also provided soft-copy of station identification tables which were used to convert the station block number to the more familiar three letter station identifier or International Civil Aviation Organization (ICAO) code name. Data was sent on 3.5-inch disks in compressed format.

The Data Comparison Process

The data comparison process involved manipulating SSM/I and ground station or "truth" databases in order to obtain paired data. Again, a data pair consists of truth and algorithm surface temperatures at the same time and place. The process can be visualized in Figure 8. The process consisted of five phases: Download, Reformat, Calculate, Match, and Compare. The first three phases were applied to both the raw SSM/I data and the ground station data. The fourth phase created the data pairs with a matching process. The fifth phase, Compare, calculates the statistics from the data pairs.

In terms of software, phases two, three, and four required a FORTRAN program to execute (see Figure 8). Eight FORTRAN programs were created to complete the data processing. With the exception of the algorithms, Comoglio and this author created all of the code for the data comparison process. Sun Sparc workstations provided the platform for phases 1-4. The comparison phase occurred on a PC using standard software.

Detailing each phase, step A consisted of transferring the raw SSM/I data on 8mm tape and the station data on 3.5 diskette to the workstations. The SSM/I data was transferred from tape directly to the workstations and a working directory using the UNIX utility program tar (Sobel, 1985). The station data was first uncompressed from a PC on the AFIT LAN, then transferred to the UNIX workstations using file transfer protocol. Station files were converted to UNIX format. The next phase in the process was reformatting.

The raw SSM/I data needed reformatting from binary to ASCII. In step B, a program (SATTIME.F) filtered the satellite date-time data for the area of interest (grid box) and

5 Phases

1. Download
2. Reformat
3. Calculate

4. Match
5. Compare

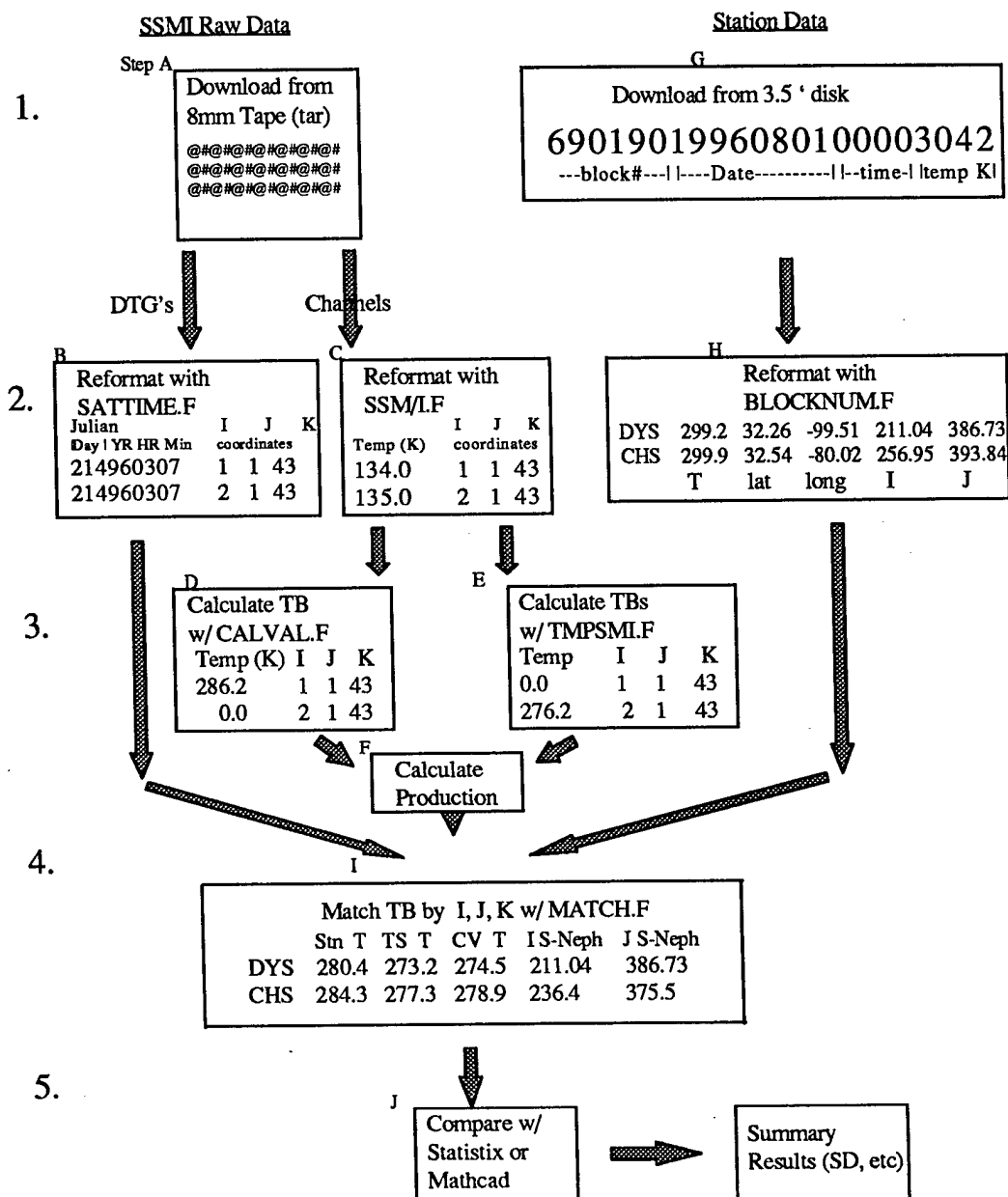


Figure 8 - Data Comparison Process

day. The output is in ASCII format in a separate file in the form shown in Table 7.

Table 7. Output from Satellite Observation Time Program

Julian Day YR HR Min	I J K coordinates
214960307	1 1 43
214960307	2 1 43 ...

In step C, another program (SSMIF) filtered the channel data files for area and day of interest, added the decimal point to the brightness temperature (see 1st column in Table 8), and reformatted the data to an ASCII file. Steps A, B, and C were complete up to this point. Steps D and E, the surface temperature calculations, were next.

Phase 3, the calculation part of the process, consisted of the actual algorithms that produce the surface temperatures. The algorithm programs produced output consisting of temperatures for each grid point such as shown in Table 8.

Table 8. Output from Surface Temperature Algorithm (CV or TS) Programs

Temp (K)	I J K coordinates
134.0	1 1 43
135.0	2 1 43 ...

With phase 3 complete, programs were run to calculate the production rates for each algorithm. The production rate represented the percent of all the grid points in the area of interest which returned a realistic temperature (step F). By this point, all the SSM/I data

had been processed and was ready for matching (Phase 4). Next, the station data needed processing to prepare for the matching phase.

After downloading and transforming from diskettes, the station data was filtered by hour of interest corresponding to the satellite observation times. Step H was accomplished by the program called BLOCKNUM.F. For one station observation at a time, the program converted the temperature and latitude/longitude to real numbers by adding the decimal point, converted latitude/longitude to a polar stereographic grid coordinate, and created a new data file ready to compare to algorithm temperature files. Output had the following items: ICAO, temperature (K), latitude, longitude, I-J-K coordinates given in the form as shown in Table 9.

Table 9. Output from Ground Station Program

ICAO	Temp (K)	Latitude (°)	Longitude (°)	I-Coord.	J-Coord.
DYS	299.2	32.26	99.51	211.04	386.73
CHS	299.9	32.54	80.02	256.95	393.84...

Phase 4 entailed the critical matching phase. Creating the algorithm-station temperature data pairs was done in three general routines by the matching program (MATCH.F):

1. For a particular day and hour, SSM/I temperatures and location were obtained by matching the coordinates of the satellite observation time with the algorithm-produced temperature and grid coordinate (files from steps B & C are combined).

2. The station observations are filtered for hour(s) of interest to obtain the corresponding temperature and grid coordinate.
3. Lastly, the algorithm surface temperature and station surface temperature are matched by grid coordinate.

A match is made if a grid with a temperature is within one grid coordinate of a ground station. Reference Figure 9 taken from Comoglio (1997). Thus, for each of the ground stations the program gathers a maximum of four surrounding points. The matching program output looks like Table 10.

Table 10. Output from Matching Program showing station, TS, and CV temperatures.

ICAO	Temp (K)	TS Temp. (K)	CV Temp. (K)	I-Super Coord.	J-Super Coord.	I-Coord.	J-Coord.
DYS	280.4	273.2	274.5	211.04	386.73	248	373
CHS	284.3	277.3	278.9	236.43	375.52	237	376

A match can be of a station temperature with just a TS temperature or a CV temperature or both. The match step produced hourly files by day, which were then manually combined into one file using a text editor. Finally, the single file was converted to ASCII format for import into various PC programs. The match step at this point was completed.

After the combined DOS files were imported into Statistix or MS-Excel, various descriptive statistics were calculated. At this point, data processing was complete. The next task was the generation of the statistics.

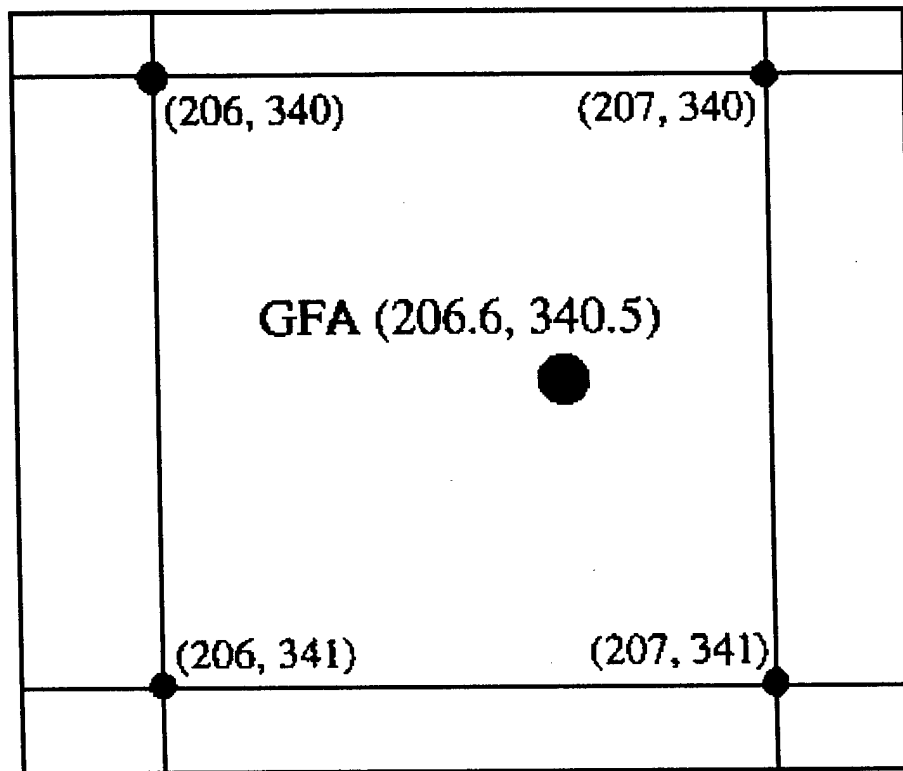


Figure 9. Polar Stereographic Grid over Malmstrom AFB (GFA)

Comparison Methods

This section outlines what was done to the large set of data pairs. With a focus on customer and operational needs, three statistics are outlined: production rate, bias, and accuracy. These three statistics clearly show algorithm differences. Lastly, data stratification or grouping is addressed.

Statistics

The appropriate statistics were mostly chosen based upon customer, i.e., AFWA, requirements. As mentioned, the DoD does not have formal performance requirements for SSM/I land surface temperatures (Glackin and Gasster, 1994).

The first descriptive statistic generated was production. This answered the first major question of the research, "How much data do the algorithms produce?" The algorithms did not produce temperatures at every grid point due to the inability to determine the land type. Production was simply the percent of grid points with a temperature.

The second statistic generated was bias. The weather forecaster using a SSM/I surface temperature product needs to know the tendency or bias of the algorithms. That is, are the retrieved temperatures usually too cold, too warm, or equal to the actual surface temperature? AFWA did not require the bias statistics because bias is calculated and corrected for at AFWA. Also called mean errors (Wilks, 1995), biases were calculated using the following formula from Kopp (1994):

$$Bias = \frac{1}{N} \sum \Delta T \quad (15)$$

where ΔT = Algorithm temperature minus station temperature
N = Number of data pairs for the particular algorithm

The last statistic generated was accuracy. Most importantly for AFWA, accuracy answers the second question, "How good are the algorithms?" As opposed to production, accuracy meant quality of the data. The Root Mean-Square Error (RMSE) defines accuracy (Kopp 1994).

$$Accuracy = \sqrt{\frac{1}{N} \sum \Delta T^2} \quad (16)$$

Accuracy referred to the average correspondence between *individual* algorithm temperature observations and the events they simulate (truth or station data). In contrast, bias (or systematic bias) measured the correspondence between *average* algorithm temperature and the *average* station temperature. The surface temperature algorithms which were consistently too warm or cold exhibit a bias, regardless of the algorithm's accuracy (Wilks, 1995). Of important note, AFWA stated an RMSE ≥ 8 K was unacceptable. Both algorithms were compared to AFWA's accuracy criteria.

Data Stratification

Since the data covered a time span of at least seven months and had global distribution, the data could be sorted or stratified either in time or space. Recall SSM/I data was available for the entire Northern Hemisphere. Spatially, the data was grouped into four regions. The first data set was over the Continental United States (CONUS). The study was then expanded to include specific areas with particular interest to the United States Department of Defense: Korean Peninsula, Saudi Arabia, and Bosnia. Descriptive statistics were calculated for three seasons: summer, fall, and winter for each region.

Unfortunately, the temperature data was too sparse to provide a color enhanced pictorial representation of brightness temperatures for the satellite passes. In addition, not all matches for one location contained pairs with both CV & TS temperatures. The matches themselves were very sparse in time (see appendices). Thus, comparative

statistics could not be shown pictorially as well. A temporal stratification was envisioned such as breaking the seasons up into weekly or daily sets. However, time did not permit such stratification, nor was AFWA concerned with one. The primary concern was seasonal and regional algorithm performance.

Summary

A complex process with many separate filter and reformatting programs was required to obtain the data pairs of truth and algorithm surface temperature. Once the data pairs were gathered, the customer driven statistics were calculated such as production, bias, and RMSE values. With all the data processed and statistics gathered the analysis process could begin.

IV. Results Analysis

Chapter Overview

This chapter has five main sections. After a short discussion about the data sets, the algorithm production is reviewed. The next section discusses the tally of data pairs. The last two sections reveal the variability of the algorithm bias and accuracy.

The sections with production, bias, and accuracy results follow a basic pattern. The first sub-section provides the overall results, e.g., grand averages. Then, the algorithm numerical differences as compared to each other are detailed. The last sub-section discusses any regional and/or seasonal patterns.

Data Sets

Twelve data sets were created – four regions each with three seasons. The four regions were the CONUS, Bosnia, Korean Peninsula, and Saudi Arabia. In reality, Bosnia was composed of some surrounding countries, which were part of the former Yugoslavia.

The number of data days for each season varied from region to region depending upon SSM/I data availability. In general, summer (1996) had 14 days, fall (1996) had 15 days, and winter (1996-1997) had 18 days (reference appendices).

Algorithm Production

The first research question addressed was, which algorithm produced more temperatures? Production is defined as the percent of temperatures calculated in the grid box (s) of interest. The important factor is the relative, i.e., TS vs CV, production rate. Absolute production rate (out of 100) is irrelevant as the grid boxes usually overlay some

ocean areas, which naturally reduce the number of land surface temperatures. The production rates are found in Table 11. Production highlights only algorithm temperature generation and not any comparison with ground observations.

Table 11. Surface Temperature Production Rate (%) for the Temperature from Sensor Microwave Imager (TS) and Calibration/Validation (CV) Algorithms.
Each region shows its approximate central latitude

Region & Latitude	SUMMER		FALL		WINTER	
	TS	CV	TS	CV	TS	CV
CONUS (39°)	33	17	28	28	18	21
BOSNIA (44°)	70	51	69	55	21	32
KOREA (37°)	84	50	40	41	8	26
SAUDI ARABIA (24°)	81	63	78	65	61	55

As the non-bold numbers indicate, TS produced more temperatures than CV in 8 out of the 12 regions. The regions varied in size and so the numbers of grid points varied from region to region. As a result, weighted averages of production were calculated. The weighted average multiplies the CONUS averages by six and the Saudi Arabian averages by two. The weighted averages for TS and CV were 49% and 42% respectively. The non-weighted production averages were also calculated. The percentages were the same - TS produced on average 49 % while CV's average production rate was 42 %. The similarity is due to the general trend of larger production percentages over regions with a smaller number of grid boxes.

Even though TS was the overall production winner, TS did show a decline in production rates from summer to winter for all regions. The TS decline was expected as the snow land type is turned off for TS thus reducing the temperature production. Even though the snow land type is turned off, TS still was competitive with CV, except for Bosnian and Korean Winters. The lack of TS decline into winter is not evident in Saudi Arabia, which is a region naturally hard-pressed to accumulate snow. Similarly, the CONUS showed little decline in production, as compared to Korea with the largest decline, as the majority of stations in CONUS were military stations concentrated in the Southern CONUS, again where snow is relatively rare. CV did not have a downward trend like TS from summer to winter except for perhaps Korea. However, the CV downward trend in Korea was not as steep as TS's Korean downward trend.

Looking at regional aspects, in general the overseas locations had more temperatures from both algorithms. More data in potential contingency locations is definitely advantageous for US military operations. Korea had both the largest (summer, TS) and smallest production rates (winter, TS). For CV, the highest production was in the Saudi Arabian Fall with the smallest production in the CONUS Summer. Saudi Arabia had the highest average production rate for all three seasons. This is a bit surprising considering Saudi Arabia's low latitude, which results in the smallest satellite coverage of the three regions (recall Figure 3). The large regional variances probably reflect the differing land types from region to region and the algorithm's ability to correctly determine those land types. Saudi Arabia has the most homogenous land type. Since the algorithms show they could identify sandy soils, large production rates were understandable in this region.

In summary, summer, non-CONUS sites, and TS produced more temperatures, but a large variance of production rates both seasonally and regionally was evident. On average, TS produced 7 % more data than CV.

Data Pair Sample Sizes

A data pair consists of the ground station temperature matched with a TS or CV algorithm produced temperature. Table 12 contains the number of data pairs by region and season.

Table 12. Number of Data Pairs for the Temperature from Sensor Microwave Imager (TS) and Calibration/Validation (CV) Algorithms

	SUMMER		FALL		WINTER	
	TS	CV	TS	CV	TS	CV
CONUS	1440	651	1157	999	1415	1330
BOSNIA	26	22	26	21	222	117
KOREA	949	465	731	533	434	796
SAUDI ARABIA	546	445	390	352	152	102

Table 12 shows TS produced more data pairs (11 out of 12 cases) than CV. With the production data in mind, one would indeed expect a large number of TS data pairs. On the other hand, with the same reasoning, one would expect the overseas regions to have a large number of data pairs. However, the small number of overseas pairs was primarily due to a less dense network of weather stations that also do not report every hour. Many

foreign stations only report the weather every three hours. Thus, fewer overseas ground weather stations means fewer potential matches.

Although not evident in the foreign numbers, the CONUS data pair numbers dipped in the fall and rose again in the winter. That trend was not entirely evident for CV because the CV's summer data set had a several days with no data. The fall reduction was most likely due to the weather station reporting code change (METAR) which occurred at this time in the US and resulted in some bad and/or lost data (Wall, 1997).

The Bosnian samples were markedly small. The small sample size was due to bad Date/Time data present on the SSM/I data tape sent from AFWA. The day number was incorrect for almost all the days used in the Bosnian region. In fact, the majority of the summer days for Bosnia had the same day number. For example, the 21 Aug 96 file contained the Julian day for 5 Aug 96. In those cases, the data was copied into the correct file assuming the Julian day matched with the correct satellite observation time. This procedure may have been incorrect as will be pointed out in the next two sections.

Bias

Bias (mean error) is the tendency for the retrieved temperature to be too high (warm) or too low (cold) compared to reality (station data). Although not as important as accuracy to AFWA as they correct for bias, bias is important for operational users of CV surface temperature products. Bias was calculated for each region by season and is shown below in Table 13.

Table 13. Bias (K) for the Temperature from Sensor Microwave Imager (TS) and Calibration/Validation (CV) Algorithms.

Bold indicates warm bias. Italics indicates CV bias > TS bias.

	SUMMER		FALL		WINTER	
	TS	CV	TS	CV	TS	CV
CONUS	-6.7	-6.6	-6.0	-3.5	-6.0	-2.7
BOSNIA	<i>-17.9</i>	<i>-18.9</i>	-6.8	-4.3	19.7	-1.2
KOREA	-10.6	-7.4	-8.6	-5.1	-5.3	-2.8
SAUDI ARABIA	-6.6	0.1	-3.5	2.3	-2.8	5.0

The boldface indicates warm bias. Table 13 shows both algorithms had a cold bias in 20 out of 24 cases. The cold bias is perhaps to due to the effect of moisture or lack moisture on the ground. If the training data sets were made over land that was more moist than normal, an average dryer land condition would provide less microwave radiation to the sensor, resulting in a smaller algorithm produced temperature. An analysis of soil moisture conditions and/or precipitation days was not accomplished. As indicated by italics, only the Bosnian-summer contained a CV bias greater than the TS bias. In all other cases, the CV bias was smaller.

For the majority of cases for both algorithms, the bias exhibited a seasonal trend of decreasing from summer to winter.

From a regional perspective, Bosnia clearly had the largest biases, cold or warm. The explanation for this probably was due to the erroneous satellite times data. The small sample sizes probably had an impact on the large biases. However, recall the Bosnian-fall

also had a very small sample size and its biases were of the same magnitude as those of the regions with large data sets. It is interesting to note, knowing that both algorithms use the same satellite time file, that the Bosnian Winter produced a CV bias comparable to other locations, but the worst bias of the whole study for the TS algorithm (19.7). The Bosnian data is certainly suspect due to the errors in the satellite times.

Another regional aspect was CV's warm bias in Saudi Arabia for all three seasons. In contrast to the previous seasonal trend, the CV warm bias increased from summer to winter. An explanation for the warm bias is possibly due to the different land types in Saudi Arabia as compared to the Western Plains and Dessert of the US where NRL gathered the land type scheme training data. To produce a warm bias, the Saudi Arabian land type would have to have a higher emissivity in reality, providing more microwave radiation to the SSM/I sensor, and in turn, providing a higher algorithm surface temperature on average.

The calculation of average biases for season and region was planned but due to the trends and large differences between the algorithm biases, averages were not calculated. Too much information would be lost in the generalization. If a weather observer or forecaster uses a TS or CV surface temperature product for one of the regions and seasons in this study, they should consult Table 13 when no other guidance is available.

In summary, both algorithms tended to produce colder temperatures on average, with the notable exception of CV in Saudi Arabia. TS temperatures exhibited the largest departures from truth. Most biases decreased from summer to winter.

Root Mean Square Error (RMSE) - Accuracy

RMSE will answer the other major question in this research, "How accurate are the TS and CV algorithms?" More specifically, did the algorithms remain below the AFWA eight-degree cut-off for acceptable accuracy? Table 14 shows RMSE value for all regions and seasons. Boldface indicates RMSE greater than or equal to 8 K (outside of acceptable accuracy limits). All twelve cases were included in the analysis. However, the Bosnian winter was suspect due the large difference between TS and CV.

Table 14. RMSE (K) for the Temperature from Sensor Microwave Imager (TS) and Calibration/Validation (CV) Algorithms. Bold indicates $\text{RMSE} \geq 8$ K.

	SUMMER		FALL		WINTER	
	TS	CV	TS	CV	TS	CV
CONUS	8.3	7.8	7.3	5.6	7.7	6.2
BOSNIA	18.5	19.4	7.5	5.3	20.5	5.2
KOREA	11.3	8.0	9.5	6.2	6.2	6.2
SAUDI ARABIA	9.2	7.4	7.4	8.0	7.4	9.7

CV was more accurate than TS in 8 out of 12 cases. The average algorithm RMSE accuracy was 9.1 and 8.1 for TS and CV, respectively. Thus in the aggregate, CV was 1 K RMSE more accurate than TS. There was no clear regional or seasonal pattern to algorithm performance as all the differences were rather close: within 2 K RMSE.

10 out of 24 cases failed to meet the accuracy criteria of < 8 K RMSE. More importantly for AFWA, TS failed to meet the criteria in 6 out of 12 cases. Note, TS was close (within 0.5 degrees) to the 8 K RMSE criteria for two cases (CONUS winter and Bosnian fall) and CV was close in one case (CONUS summer). CV failed the accuracy criteria in 4 out of 12 cases. In other words, CV met the accuracy $(8/12 - 6/12)$ 16 % more often than TS. Note, if the accuracy criteria was < 8 K RMSE, two CV scores (Korean summer and Saudi Arabian fall) would be changed to acceptable, increasing the acceptance rate by 50%.

Seasonally, in summer (excluding Bosnia) TS was less accurate than CV, and in fact never met the criteria. Summer was also the least accurate season for CV. There was no consistent trend from summer to winter for either algorithm.

In short, CV was more accurate, more often than TS. CV met the accuracy criteria 16 % more often than TS and beat TS in 75% of all the cases. On average, CV was 1 K RMSE more accurate than TS.

Summary

In terms of production, TS produced 7 % more surface temperatures than CV. On the other hand, TS was less accurate than CV. On average, CV was 1.0 K RMSE more accurate than TS and met the accuracy criteria 16 % more often than TS. Both algorithms mostly exhibited a cold bias, but CV displayed a warm bias in Saudi Arabia.

V. Summary and Recommendation

Summary

With a large comparative study, the present research provided information on AFWA's two main questions about the TS and CV algorithms. Concerning amounts of data, TS on average produced 7 % more surface temperatures than CV. The production percentages varied greatly by region and season.

The accuracy numbers did not vary as much by region and season. On average, CV is 16 % more accurate in meeting the AFWA accuracy criteria of $RMSE < 8\text{ K}$. CV had an average 1 K RMSE better accuracy than TS. CV met or beat TS in 75 % of the cases.

It is interesting to note the bias behavior of the two algorithms. An overall cold bias is prevalent but warm biases did exist as for CV in Saudi Arabia. Biases generally declined in winter.

Data Processing Recommendations

Several or all of the eight FORTRAN program types could be combined into one program. Certainly, the Reformat Phase (steps B & C and H) programs could be combined. Combining would save much processing time. Similarly, a program could be written to automatically combine all the daily match files into the single file with all the data pairs (last part of Phase 4). Doing so would save time and eliminate the manually intensive cut and paste operations currently needed in the last data processing step.

Research Recommendations

A performance comparison should be made of over the various land types. In addition, the effect of clouds and precipitation on algorithm accuracy could be investigated. A correlation study could be done to match up weather observations of surface temperature, clouds and precipitation with algorithm produced temperatures.

For CV, a fifth algorithm is available which is a combination of all the data used in the regression analysis. The fifth algorithm can be used if the original four land types cannot be determined (McFarland, 1991). The effect of the fifth algorithm on CV production and accuracy would be interesting. Similarly, contact the CV contractor should be done to determine if any new CV algorithms for other land types are available.

Concerning the present study's production results, CV produced temperatures for approximately 90 % of all the grid points on 21 Oct 96. No other day for either algorithm had such a high rate. A cause could not be determined and is left for further study.

Finally, a regression analysis could be done on this study's data pairs to derive new coefficients and compare them to the current coefficients used in both algorithms. This study's database is by far larger (>13,300 pairs) than the studies performed at AFWA (~1000 data pairs) (Kopp, 1997) and the original CV validation study performed in 1987 (~1800 pairs) (McFarland, 1991). Separate algorithms could be generated for each location and season analyzed in this study.

Appendix A - Summer CONUS Matches

Julian Day	00Z	01Z	02Z	03Z	04Z	05Z	06Z	07Z	08Z	09Z	10Z	11Z	12Z	13Z	14Z	15Z	16Z	17Z	18Z	19Z	20Z	21Z	22Z	23Z	sum
214 1-Aug		32		58		22																			112
218 5-Aug																									
219 6-Aug	62				59																				121
220 7-Aug	57				73	67																			197
221 8-Aug	59	17				38																			114
222 9-Aug		20			60																				80
225 12-Aug		60																							60
226 13-Aug		70			2																				72
227 14-Aug																									0
228 15-Aug	37			36	4																				77
232 19-Aug		12	3		27							89	67												198
233 20-Aug		44		67	22																				133
239 26-Aug		22		42	23	12																			99
240 27-Aug		40		58	79																				177
14 Days																									TOTAL 1440

Appendix B - Fall CONUS Matches

Julian Day	00Z	01Z	02Z	03Z	04Z	05Z	06Z	07Z	08Z	09Z	10Z	11Z	12Z	13Z	14Z	15Z	16Z	17Z	18Z	19Z	20Z	21Z	22Z	23Z	sum
290	16-Oct	24		61		81																			166
291	17-Oct	48			62																				110
292	18-Oct		1	4	57																				62
295	21-Oct	42			67	11						96			33										249
296	22-Oct	72		12		8																			92
297	23-Oct																								
298	24-Oct																								
299	25-Oct	48		62																					110
302	28-Oct																								
303	29-Oct	1		4								34		77	22										138
304	30-Oct																								
305	31-Oct	13		60	1	42																			116
309	4-Nov	28				24						4		58											114
310	5-Nov	43	4	14	4	79																			144
311	6-Nov																								
15 Days																							TOTAL		1301

Appendix C - Winter CONUS Matches

Julian Day	00Z	01Z	02Z	03Z	04Z	05Z	06Z	07Z	08Z	09Z	10Z	11Z	12Z	13Z	14Z	15Z	16Z	17Z	18Z	19Z	20Z	21Z	22Z	23Z	sum
30	30-Jan	68	12	54																					134
31	31-Jan		20	7	61																				88
34	3-Feb		37		55																				92
35	4-Feb		53	17	35																				105
36	5-Feb	12			10	38																			60
37	6-Feb	5				60																			65
38	7-Feb	61																							61
41	10-Feb			18	29																				47
42	11-Feb		46	1	62																				109
43	12-Feb		22	74	60																				156
44	13-Feb	22	11	28	68	20																			149
45	14-Feb			3	69	33	3																		108
49	18-Feb		20	61	40																				121
51	20-Feb		50	8	1																				59
52	21-Feb		6			45																			51
55	24-Feb	64		12	61	5																			142
57	26-Feb																								
58	27-Feb		8		39	38																			85
18 Days																									TOTAL 1632

Appendix D - Summer Bosnian Matches

Julian Day	00Z	01Z	02Z	03Z	04Z	05Z	06Z	07Z	08Z	09Z	10Z	11Z	12Z	13Z	14Z	15Z	16Z	17Z	18Z	19Z	20Z	21Z	22Z	23Z	sum
214	1-Aug																								
218	5-Aug																								
219	6-Aug																26								26
220	7-Aug																								
221	8-Aug																								
222	9-Aug																								
225	12-Aug																								
226	13-Aug																								
227	14-Aug																								
228	15-Aug																								
232	19-Aug																								
233	20-Aug																								
239	26-Aug																								
240	27-Aug																								
14 Days																							TOTAL		26

Appendix E - Fall Bosnian Matches

Julian Day	00Z	01Z	02Z	03Z	04Z	05Z	06Z	07Z	08Z	09Z	10Z	11Z	12Z	13Z	14Z	15Z	16Z	17Z	18Z	19Z	20Z	21Z	22Z	23Z	sum
290	16-Oct																								
291	17-Oct																								
292	18-Oct																								
295	21-Oct																								
296	22-Oct																								
297	23-Oct																								
298	24-Oct																								
299	25-Oct																								
302	28-Oct																								
303	29-Oct																								
304	30-Oct																								
305	31-Oct																								
309	4-Nov																37								37
310	5-Nov																								
311	6-Nov																								
15 Days																							TOTAL		37

Appendix F - Winter Bosnian Matches

Julian Day	00Z	01Z	02Z	03Z	04Z	05Z	06Z	07Z	08Z	09Z	10Z	11Z	12Z	13Z	14Z	15Z	16Z	17Z	18Z	19Z	20Z	21Z	22Z	23Z	sum
30	30-Jan						11									211									222
31	31-Jan																								
34	3-Feb																								
35	4-Feb																								
36	5-Feb																								
37	6-Feb																								
38	7-Feb																								
41	10-Feb																								
42	11-Feb																								
43	12-Feb																								
44	13-Feb																								
45	14-Feb																								
49	18-Feb																								
51	20-Feb																								
52	21-Feb																								
55	24-Feb																								
57	26-Feb																								
58	27-Feb																								
18 Days																								TOTAL	222

Appendix G - Summer Korean Matches

Julian Day	00Z	01Z	02Z	03Z	04Z	05Z	06Z	07Z	08Z	09Z	10Z	11Z	12Z	13Z	14Z	15Z	16Z	17Z	18Z	19Z	20Z	21Z	22Z	23Z	sum
214 1-Aug			118																						118
218 5-Aug			118																						118
219 6-Aug				2																					2
220 7-Aug			124																						124
221 8-Aug																									
222 9-Aug																									
225 12-																									
226 13-			139																						139
227 14-																									
228 15-		7	16																						23
232 19-				80																					80
233 20-			116																						116
239 26-		115																							115
240 27-		114																							114
14 Days																							TOTAL		949

Appendix H - Fall Korean Matches

Julian Day	00Z	01Z	02Z	03Z	04Z	05Z	06Z	07Z	08Z	09Z	10Z	11Z	12Z	13Z	14z	15Z	16z	17Z	18z	19Z	20Z	21Z	22Z	23Z	sum
290	16-Oct		80																						80
291	17-Oct																								
292	18-Oct			80																					80
295	21-Oct								85						1										86
296	22-Oct		119																						119
297	23-Oct																								
298	24-Oct																								
299	25-Oct		100																						100
302	28-Oct																								
303	29-Oct												81												81
304	30-Oct																								
305	31-Oct		99																						99
309	4-Nov												99												99
310	5-Nov																								
311	6-Nov																								
15 Days																							TOTAL		744

Appendix I - Winter Korean Matches

Julian Day	00Z	01Z	02Z	03Z	04Z	05Z	06Z	07Z	08Z	09Z	10Z	11Z	12Z	13Z	14Z	15Z	16Z	17Z	18Z	19Z	20Z	21Z	22Z	23Z	sum
30	30-Jan		83																						83
31	31-Jan		80																						80
34	3-Feb		45																						45
35	4-Feb																								
36	5-Feb		86																						86
37	6-Feb		94																						94
38	7-Feb																								
41	10-Feb																								
42	11-Feb			4																					4
43	12-Feb		47																						47
44	13-Feb																								
45	14-Feb																								
49	18-Feb		78																						78
51	20-Feb																								
52	21-Feb		109																						109
55	24-Feb		99																						99
57	26-Feb																								
58	27-Feb		108																						108
18 Days																							TOTAL		833

Appendix J - Summer Saudi Arabian Matches

Julian Day	00Z	01Z	02Z	03Z	04Z	05Z	06Z	07Z	08Z	09Z	10Z	11Z	12Z	13Z	14Z	15Z	16Z	17Z	18Z	19Z	20Z	21Z	22Z	23Z	sum
214	1-Aug				25																				25
218	5-Aug			72																					72
219	6-Aug			52					2																54
220	7-Aug			21																					21
221	8-Aug			6	4																				10
222	9-Aug				10																				10
225	12-Aug			74																					74
226	13-Aug			69																					69
227	14-Aug																								
228	15-Aug			18																					18
232	19-Aug															87									87
233	20-Aug			65																					65
239	26-Aug																								
240	27-Aug			43																					43
14 Days																							TOTAL		548

Appendix K - Fall Saudi Arabian Matches

Julian Day	00Z	01Z	02Z	03Z	04Z	05Z	06Z	07Z	08Z	09Z	10Z	11Z	12Z	13Z	14Z	15Z	16Z	17Z	18Z	19Z	20Z	21Z	22Z	23Z	sum
290 16-Oct			35																						35
291 17-Oct				59																					59
292 18-Oct				70																					70
295 21-Oct			4					59							4										67
296 22-Oct			5	2																					7
297 23-Oct																									
298 24-Oct																									
299 25-Oct				53																					53
302 28-Oct																									
303 29-Oct			14					10							15										39
304 30-Oct																									
305 31-Oct					12																				12
309 4-Nov															52										52
310 5-Nov																									
311 6-Nov																									
15 Days																							TOTAL		394

Appendix L - Winter Saudi Arabian Matches

Julian Day	00Z	01Z	02Z	03Z	04Z	05Z	06Z	07Z	08Z	09Z	10Z	11Z	12Z	13Z	14z	15Z	16z	17Z	18z	19Z	20Z	21Z	22Z	23Z	sum
30	30-Jan			8	1																				9
31	31-Jan				10																				10
34	3-Feb				6																				6
35	4-Feb																								
36	5-Feb																								
37	6-Feb			4																					4
38	7-Feb			13																					13
41	10-Feb																								
42	11-Feb				67																				67
43	12-Feb																								
44	13-Feb																								
45	14-Feb			19																					19
49	18-Feb																								
51	20-Feb																								
52	21-Feb				59																				59
55	24-Feb			8																					8
57	26-Feb																								
58	27-Feb				2																				2
18 Days																							TOTAL		197

Bibliography

Chen, Daoyi and Brutsaert Engman, "Spatial Distribution and Pattern Persistence of Soil Moisture and Temperature over Prairie from Remote Sensors," Remote Sensing of the Environment: 61, (1997)

Comoglio, Ronald L. A Validation Study of the SSM/I Temperature Algorithm and Comparison with the CV Land Surface Temperatures. MS Thesis, AFIT/GM/ENP/97M-02. School of Engineering Physics, Air Force Institute of Technology (AU), Wright -Patterson AFB OH, February 1997.

Conway, Thomas G., "Improved Remote Heat Sensing," Mechanical Engineering, 88-89 (May 1997)

Cooper, Pat, "Air Force Launches DMSP Weather Satellite Built By Lockheed Martin." WWWeb, <http://www.lmsc.lockheed.com/newsbureau/pressreleases/9710.html> (23 Aug 97).

"Defense Meteorological Satellite Program (DMSP)." WWWeb, [http://www.laafb.af.mil/SMC/PA/ Fact Sheets /dmsp_fs.htm](http://www.laafb.af.mil/SMC/PA/Fact%20Sheets/dmsp_fs.htm). (23 Aug 97)

Duel, Greg, "Defense Meteorological Satellite Program (DMSP)." WWWeb, [http://microwave.msfc.nasa.gov: 5721/source_documents/dmsp_f13.html](http://microwave.msfc.nasa.gov:5721/source_documents/dmsp_f13.html)

Fett, Robert W., and others, "Application of Hypermedia and Expert System Technology to Navy Environmental Satellite Image Analysis," Bulletin of the American Meteorology Society, Vol. 78-9: (September 1997)

Fuhrhop, Rolf, and Clemens Simmer, "SSM/I Brightness Temperature Corrections for Incidence Angle Variations," Bulletin of the American Meteorology Society, 13: 246-254 (February 1996).

Glackin, David L. and Samuel Gasster, Earth Remote Sensing, The Aerospace Corporation, 1994

Harris Corp., "SSM/I Algorithm." Electronic Message. 201918Z 14 Oct 97.

Hesser, William A., Global Evaluation of Special Sensor Microwave/Imager Ocean Surface Wind Speed Retrieval Algorithms for the Period September 1991-April 1992, MS Thesis, Naval Postgraduate School, Monterey CA, June 1995

Hollinger, J.P.. SSMI Project Summary Report, Naval Research Laboratory, Washington DC, 20 April 1983

- Janssen, Michael A., Atmospheric Remote Sensing by Microwave Radiometry, New York: John Wiley and Sons, Inc., 1993.
- Kopp, Thomas J. The Air Force Global Weather Central Surface Temperature Model, AFGWC/TN-95/004. Offutt AFB NE: AFGWC, December 1995
- Kopp, Thomas J. Team Chief, Meteorological Models Cloud Team, AFGWC, Offutt AFB NE. Meeting. Feb 97.
- Kopp, Thomas J. 'Application of SSM/I to Real-time Automated Satellite Nephanalysis Model', 7th Conference of Satellite Meteorology and Oceanography, American Meteorology Society, 1994
- Macelloni, G., and others, "Spaceborne Microwave Radiometry of Land Surfaces," SPIE: 2313, 129-135 (1994)
- MacFarland, Marshall J. and others, "Land Parameter Algorithm Validation and Calibration," in DMSP Special Sensor Microwave/Imager Calibration/Validation. Final Report, Volume II, 9-40
- McIlveen, Robin, Basic Meteorology - A Physical Outline, Berkshire, England: Van Nostrand Reinhold Company, 1986
- Prata, A.J., "Land Surface Temperature Determination from Satellites," Advanced Space Research Vol.14: 15-26 (1994)
- Rees, W. G., Physical Principles of Remote Sensing, Cambridge, England: Cambridge University Press, 1990
- Sobell, Mark G, A Practical Guide to UNIX System V, Reading MA: Benjamin/Cummings Publishing Co., Inc., 1985
- Spiegel, Murray R., Mathematical Handbook of Formulas and Tables - Schaum's Outline Series, New York: McGraw-Hill, Inc., 1994
- Ulaby, Fawwaz T. and others. Microwave Remote Sensing: Active and Passive, Volume 1, Reading MA: Addison-Wesley Publishing Company, 1981.
- Wall, Roy L., Meteorologist, Air Force Combat Climatology Center, Ashville NC. Telephone interview. 3 November 1997.
- Wilks, Daniel S., Statistical Methods in the Atmospheric Sciences, San Diego; Academic Press, 1995.

Vita

Captain Harris was born in Pekin, Illinois, on May 4, 1965, but was raised in Framingham, Massachusetts. He attended Framingham South High School and graduated in 1983 with honors in mathematics.

In September 1984, Captain Harris entered the Reserve Officer Training Corps (ROTC) at Lyndon State College, Lyndonville, Vermont. He subsequently graduated from college in May 1988 with a Bachelor of Science Degree in Meteorology and was commissioned a second lieutenant in the United States Air Force on May 14, 1988.

After commissioning, Captain Harris was assigned to Detachment 3, 5th Weather Squadron, Fort Bragg, North Carolina in January 1989. Captain Harris served with distinction with the 7th Special Forces Group (Airborne) during Operation JUST CAUSE in Panama.

In Jan 93, Captain Harris was assigned to Headquarters, Air Weather Service (HQ AWS), Directorate of Operations, Training Division, Scott Air Force Base, Illinois. From Feb 93 to Jan 95, he was the training system designer and manager for the Automated Weather Distribution System, Small Tactical Terminal and several other new weather equipment acquisitions. From Jan 95 to Aug 95, he was the project officer for the future fielding of the Tactical Weather Radar. From Aug 95 to Aug 96, he was the Chief of Acquisition Policy and Resource Management branch.

In Aug 95, Capt. Harris was a distinguished graduate of Squadron Officer School, Maxwell AFB, Alabama. He earned a Masters in Business Administration from Southern Illinois University - Edwardsville in May 96.

Captain Charles H. Harris arrived Aug 96 at the AF Institute of Technology to pursue a Masters in Meteorology degree. He has a follow on assignment as the Chief of Scientific Services, 7th Weather Squadron, Heidelberg, Germany.

Captain Harris is married to the former Sheryl Ann Stuart of Sheffield, Vermont. They have a daughter Caitlin (b: 11 Dec 91) and son Alex (b: 28 Apr 96).

Permanent Address: 3 Rolling Drive
Framingham MA 01701

REPORT DOCUMENTATION PAGE			Form Approved OMB No. 0704-0188
<small>Public reporting burden for this collection of information is estimated to average 1 hour per response, including the time for reviewing instructions, searching existing data sources, gathering and maintaining the data needed, and completing and reviewing the collection of information. Send comments regarding this burden estimate or any other aspect of this collection of information, including suggestions for reducing this burden, to Washington Headquarters Services, Directorate for Information Operations and Reports, 1215 Jefferson Davis Highway, Suite 1204, Arlington, VA 22202-4302, and to the Office of Management and Budget, Paperwork Reduction Project (0704-0188), Washington, DC 20503.</small>			
1. AGENCY USE ONLY (Leave blank)	2. REPORT DATE Mar 98	3. REPORT TYPE AND DATES COVERED Master's Thesis	
4. TITLE AND SUBTITLE EVALUATION OF SATELLITE MICROWAVE DERIVED SURFACE TEMPERATURE ALGORITHMS FOR THE PERIOD AUGUST 1996 TO FEBRUARY 1997		5. FUNDING NUMBERS	
6. AUTHOR(S) Charles H. Harris, Captain, USAF			
7. PERFORMING ORGANIZATION NAME(S) AND ADDRESS(ES) Air Force Institute of Technology 2750 P Street WPAFB OH 45433-7765		8. PERFORMING ORGANIZATION REPORT NUMBER AFIT/GM/ENP/98M-04	
9. SPONSORING/MONITORING AGENCY NAME(S) AND ADDRESS(ES) Thomas J. Kopp, Branch Chief AFWA/DNXM 106 Peacekeeper Dr. STE 2N3, Offutt AFB NE 68113-4039		10. SPONSORING/MONITORING AGENCY REPORT NUMBER	
11. SUPPLEMENTARY NOTES			
12a. DISTRIBUTION AVAILABILITY STATEMENT Approved for public release; distribution unlimited		12b. DISTRIBUTION CODE	
13. ABSTRACT (Maximum 200 words) <p>The Air Force Weather Agency (AFWA) has two operational algorithms that derive surface temperatures from microwave observations taken by the Special Sensor Microwave Imager (SSM/I) which rides aboard space platforms of the Defense Meteorological Satellite Program (DMSP). The algorithm called Temperature from Satellite Microwave Imager (TS) is used to analyze global cloud coverage. The second algorithm is fittingly called Calibration/Validation (CV), as it was the algorithm used to calibrate and validate the first SSM/I in 1987. Multiple linear regression defined the algorithms from empirically gathered brightness temperatures and simultaneous surface temperatures. The key questions were how much data do these algorithms produce and how accurate is it.</p> <p>These questions were answered with a multi-seasonal comparative study over four locations. The study matched algorithm outputs to conventional weather station temperature readings. Over 13,300 data pairs were generated from the 1996 summer and fall and 1996-1997 winter for the Continental United States, Bosnia, Korea, and Saudi Arabia.</p> <p>The results show TS produced on average 7 % more surface temperatures than CV. CV met AFWA's accuracy criteria 16 % more often than TS. On average, CV was 1.0 degree Celsius more accurate than TS. The study generated bias tables for all locations and seasons.</p>			
14. SUBJECT TERMS surface temperature, algorithms, microwaves, satellite meteorology		15. NUMBER OF PAGES 90	
		16. PRICE CODE	
17. SECURITY CLASSIFICATION OF REPORT UNCLASSIFIED	18. SECURITY CLASSIFICATION OF THIS PAGE UNCLASSIFIED	19. SECURITY CLASSIFICATION OF ABSTRACT UNCLASSIFIED	20. LIMITATION OF ABSTRACT UL